Temporal patterns of thermal emission directionality of crop canopies

Huaguo Huang,[1,2] Qinhuo Liu,[2] Wenhan Qin,[2,3] Yongming Du,[2] and Xiaowen Li[2]

Received 15 June 2010; revised 8 January 2011; accepted 13 January 2011; published 29 March 2011.

[1] Many field experiments have observed significant temporal variations of thermal infrared (TIR) emission directionality, making it necessary to explain this phenomenon quantitatively to exploit potential applications of the directional remotely sensed TIR observation. The main objective of this paper is to determine when and how the significant directional effect appears. Two models, TRGM and Cupid, are linked to simulate the temporal variations of directional brightness temperature $T_B(\theta)$ of crop canopies, including winter wheat and summer corn. Two indicators are defined: (1) $\Delta T_{B,AVG}$ representing the mean difference between nadir $T_B(0)$ and off-nadir $T_B(55)$ and (2) $\Delta T_{B,STD}$ representing the standard deviation of $T_B(55)$ for different view azimuth angles. Simulation results show that the highest $\Delta T_{B,AVG}$ of up to 4°C appears mostly at midday (1200–1300 LT), while the lowest $\Delta T_{B,AVG}$ appears mostly in the early morning (0700–0800 LT) or late afternoon (1700–1800 LT). The $\Delta T_{B,STD}$ is about one third of $\Delta T_{B,AVG}$ and should not be neglected given its considerable value at around 1400 LT. This trend has been proven through field measurements at both wheat and corn sites. The major factors affecting the trend are also identified using sensitivity analysis. Among the major factors, soil water content, LAI, and solar radiation are the three most significant factors, whereas the wind speed and air temperature have a larger effect on $\Delta T_{B,AVG}$ than air humidity. It is interesting that $\Delta T_{B,AVG}$ reaches a maximum value when the LAI is around 0.8. Further analysis shows that $\Delta T_{B,AVG}$ is related to soil surface net radiation, which will be useful in net radiation estimation.

Citation: Huang, H., Q. Liu, W. Qin, Y. Du, and X. Li (2011), Temporal patterns of thermal emission directionality of crop canopies, *J. Geophys. Res.*, *116*, D06114, doi:10.1029/2010JD014613.

1. Introduction

[2] Land surface temperature is of great interest in various research areas, including the assessment of water and energy budgets at the biosphere-atmosphere interface. In climate studies or agricultural meteorology, it is vitally important for net surface radiation calculation, which is one of the main components of the driving force for surface energy balance. This temperature depends strongly on micrometeorological conditions (i.e., wind speed, air temperature, and radiation intensity) and soil moisture status. These conditions allow monitoring of crop growth potentials [*Jackson et al.*, 1979; *Jackson et al.*, 1977; *Moran et al.*, 1994] and estimation of surface fluxes [*Bastiaanssen et al.*, 1998; *Choudhury et al.*, 1986; *Chehbouni et al.*, 2001a; *Mauser and Schadlich*, 1998; *Norman et al.*, 2000; *Rivas and Caselles*, 2004; *Seguin et al.*, 1994] from remotely sensed large-scale TIR data.

[3] However, surface radiative temperature measured using remote sensors may vary significantly with different view angles, a fact which was discovered as early as in the mid-1960s [*Fuchs et al.*, 1967; *Monteith and Szeicz*, 1962]. Further observations confirmed this angular effect for different surface types [*Balick and Hutchinson*, 1986; *Balick et al.*, 1987; *Dozier and Warren*, 1982; *Lagouarde et al.*, 1995, 2000, 2004; *Liu et al.*, 2000, 2001; *McAtee et al.*, 2003; *Menenti et al.*, 2001; *Parsons*, 1985; *Paw U et al.*, 1989; *Smith et al.*, 1997b]. According to the experimental results presented by *Paw U* [1992], the directional radiative temperature of row crop canopies can vary up to 13 K, thus it is not possible to evaluate surface fluxes accurately using a single directional surface radiative temperature measured by remote sensors. This issue has gained importance as more and more satellite sensors with large swath angles, including the Moderate Resolution Imaging Spectroradiometer (MODIS), the Advanced Very High Resolution Radiometer (AVHRR) series, and the Along

[1]Key Laboratory for Silviculture and Conservation of Ministry of Education, Beijing Forestry University, Beijing, China.
[2]State Key Laboratory of Remote Sensing Science, Institute of Remote Sensing Applications, Chinese Academy of Sciences, Beijing Normal University, Beijing, China.
[3]SSAI, NASA Goddard Space Flight Center, Greenbelt, Maryland, USA.

Copyright 2011 by the American Geophysical Union.
0148-0227/11/2010JD014613

Track Scanning Radiometer (ATSR, AATSR) have come into use. In recent years, researchers have developed a series of directional thermal radiation models for homogeneous canopies [*François et al.*, 1997; *Liu et al.*, 2003; *Verhoef et al.*, 2007], row crop canopies [*Du et al.*, 2007; *Kimes et al.*, 1980; *Sobrino and Caselles*, 1990; *Yan et al.*, 2001; *Yu et al.*, 2004], and 3-D surfaces [*Guillevic et al.*, 2003; *Liu et al.*, 2007; *Luquet et al.*, 2003; *Smith et al.*, 1997a]. All these models require component temperatures as input to predict the directional brightness temperature, denoted as $T_B(\theta)$.

[4] Both $T_B(\theta)$ and the distribution of component temperatures in a canopy vary with time [*Humes et al.*, 1994]. *Chehbouni et al.* [2001b] discussed seasonal variations of $T_B(\theta)$ by analyzing the radiative temperature differences between nadir and off-nadir directions during the growth season of semiarid grasslands. The results of his study indicate that differences between nadir $T_B(0)$ and off-nadir $T_B(55)$ could rise to 5 K. Such differences are highly correlated with surface soil moisture and vegetation biomass; they also exhibit different seasonal cycles. *Guillevic et al.* [2003] demonstrated the diurnal $T_B(\theta)$ variations of about 2–3 K from 6 to 13 h with the directional brightness temperature data collected by *Kimes and Kirchner* [1983] in a cotton canopy.

[5] Therefore, it is necessary to determine the temporal variations of $T_B(\theta)$, which can be used to normalize directional effects of remotely sensed TIR data to provide accurate upwelling radiation. Moreover, the directional effect contains potential information that can be used to derive surface flux or extract canopy structural parameters. For example, *Kimes* [1983] investigated the feasibility of extracting component temperature and canopy structural information from multiple view angle measurements of temperature over crop canopies. *Chehbouni et al.* [2001a] found that accurate dual angles of measured directional radiative temperatures could be used to estimate sensible heat flux of sparse vegetation canopies. *Timmermans et al.* [2009] applied an inversion method to retrieve four canopy component temperatures from directional brightness temperatures.

[6] However, field experiments are usually carried out within a limited period under limited conditions, making it difficult to obtain $T_B(\theta)$ continually under all kinds of environmental conditions. Furthermore, observations of $T_B(\theta)$ have been taken with broadband instruments, but the satellite sensors (e.g., MODIS) are mostly narrowband. Thus, the temporal and spectral effects of the directional brightness temperature have to be estimated in order to improve surface temperature retrieval from remote sensing data. Several methods have already been adopted to predict $T_B(\theta)$ at a given point in time space by using energy budget and microclimate models directly [*Belot et al.*, 2004; *Luquet et al.*, 2003, 2004; *Merlin and Chehbouni*, 2004; *Norman et al.*, 1990; *Paw U*, 1991]. Recently, *Saux-Picart et al.* [2009] developed a one-dimensional (1-D) three source land surface model SEtHyS_Savannah coupling with a radiative transfer model [*François*, 2002] and simulated TIR temperatures at field scale. *van der Tol et al.* [2009] developed an integrated radiative transfer and energy balance model (SCOPE) that can reproduce temporal variations of directional radiance for homogeneous canopies. However, more work should be conducted to model the temporal variations of $T_B(\theta)$ of heterogeneous crop canopies under different environmental conditions; this gap is therefore the purpose of this study.

[7] In section 2, the simulation and analysis method are introduced in detail. In section 3, two field sites, in which the directional temperature observations were carried out, are briefly described, with the experimental setup and data processing presented in section 4. In section 5, TRGM performance is examined. In section 6, we evaluate the two-model method from three aspects. Based on model simulations and field measurements, the seasonal and diurnal variations of $T_B(\theta)$ as well as the influences of different factors on the temporal variations of $T_B(\theta)$ are presented in section 7. Following in section 8 are discussions on the temporal patterns and limitations. Finally, we present conclusions in section 9.

2. Methodology

[8] A two-model linking strategy is adopted to simulate the temporal variations of thermal emission directionality of crop canopies [*Huang et al.*, 2010]. A brief introduction of the two models, Cupid [*Huang et al.*, 2006; *Norman et al.*, 1990] and TRGM [*Liu et al.*, 2007], is presented below for readers who are not familiar with them.

2.1. TRGM

[9] TRGM is an extension of RGM [*Qin and Gerstl*, 2000] for TIR domain [*Liu et al.*, 2007], which can scale component temperatures up to $T_B(\theta)$ for the entire canopy. Here, component refers to sunlit/shaded foliage or soil. TRGM has been comprehensively validated by *Liu et al.* [2007]. The major requirements to drive TRGM include 3-D virtual scene file, component temperatures, component emissivity, incident sky radiation, and sensor viewer settings. The component emissivities are defined for several narrow bands and one broad band with default values (0.98 for leaf and 0.95 for soil).

[10] A 3-D structure with detailed component temperature distribution enables TRGM to simulate more realistic thermal radiation regime and emission directionality than geometric optics and radiative transfer models. On the other hand, multiple component temperatures, which are difficult to measure in the field, are input for TRGM. Thus, TRGM has to be linked with a model, such as the Cupid model, that can simulate constant variations in time and space of component temperatures of vegetation canopy.

2.2. Cupid Model and Its Extension

[11] The Cupid model [*Norman*, 1979, 1982; *Norman et al.*, 1990] is a comprehensive soil-vegetation-atmosphere transfer (SVAT) model that simulates complete radiation, convection/turbulence, and hydrologic processes occurring at the soil/canopy interface [*Kustas and Anderson*, 2009]. The Cupid model is chosen because it accounts for LAD and its effect on leaf temperature distribution more accurately than other models, such as SHAW [*Flerchinger et al.*, 1998] and ISBA [*Noilhan and Mahfouf*, 1996]. Its processing time is faster than 3-D models such as the DART EB [*Gastellu-Etchegorry*, 2008]. There are two boundary conditions to compute the profiles of temperature/moisture/wind above,

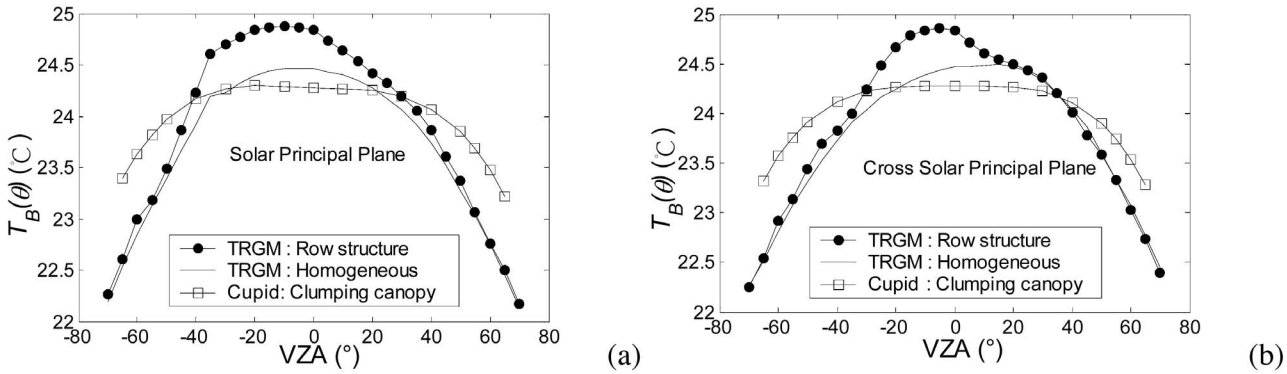

Figure 1. Comparisons of $T_B(\theta)$ simulation results for the TRGM model using row structure or homogeneous canopy and the Cupid model using homogeneous canopy corrected by a clumping index (0.54 estimated from [*Kustas and Norman*, 1999]): (a) $T_B(\theta)$ in solar principal plane and (b) $T_B(\theta)$ cross solar principal plane. LAI is 1.4, canopy height is 0.25 m, row spacing is 0.15 m, row width is 0.055 m, Sun position is (39°, 149°), sunlit and shaded soil temperatures are 28.4°C and 25.0°C, and mean leaf temperature is 22.0°C.

within, and below the canopy iteratively, namely, the bottom of the root zone and reference height above the canopy [*Norman*, 1982]. The canopy is divided into layers with ten leaf angle classes. Soil is divided into layers starting at the soil surface and ending at a sufficient depth so that changes are insignificant over time (at least 0.5 m).

[12] Cupid can model $T_B(\theta)$ based on Apparent Directional Infrared Temperature equations [*Norman et al.*, 1990] without considering the row structure. It is coherent with our simulation results that the Cupid model underestimates the hot spot effect in both solar principal plane and its cross plane and overestimates the $T_B(\theta)$ at the off-nadir view for row structure crop canopies (Figure 1). This is the reason for the need for TRGM instead of using Cupid alone for row structure canopies. Moreover, this version of Cupid only provides mean soil surface temperature and is only suitable for horizontally homogeneous canopy, which cannot satisfy the basic requirement of TRGM. At least the shaded part and sunlit part should be separated. Therefore, based on the most recent version of the Cupid model from the Website (http://www.soils.wisc.edu/~norman/cupid/), we proposed an extension that allows us to calculate the temperatures of sunlit and shaded soil surfaces simultaneously using the difference in net radiance and evaporation rate between the shaded and sunlit soil [*Huang et al.*, 2006]. Finally, the extended Cupid model can simulate detailed leaf temperatures and two soil temperatures that meet the basic needs of TRGM. In this paper, Cupid uses broadband emissivity (8–14 μm) with default values of 0.98 and 0.95 for leaf and soil, respectively.

2.3. Link Steps for Simulation

[13] There are three main steps to link Cupid and TRGM. First, Cupid predicts leaf temperature profiles and sunlit and shaded soil temperatures on an hourly or half-hourly basis. Cupid has a 1-D canopy structure with several thin leaf layers with an equivalent leaf area volume density and several soil layers. In simulating temperatures for ten different leaf angles and two soil surfaces (sunlit/shaded part) with a single run, Cupid can appear to be used in a quasi-2-D structure. These temperatures are rearranged per layer and sunlit fraction and stored in a file THERMAL.IN. Then, according to the measured canopy structural parameters, the virtual scene file POLY.IN of a crop canopy is generated with MELS [*Qin and Gerstl*, 2000]. Based on the POLY.IN and THERMAL.IN, TRGM simulates the $T_B(\theta)$. POLY.IN stores 3-D coordinates and THERMAL.IN saves the quasi-2-D temperature profiles; hence, each polygon in POLY.IN is identified in THERMAL.IN by the layer number, leaf angle, and sunlit fraction.

2.4. Definition of Directional Indicators for $T_B(\theta)$

[14] Previous works have shown that the difference between nadir $T_B(0)$ and off-nadir $T_B(55)$ [*Chehbouni et al.*, 2001b] is a useful indicator for $T_B(\theta)$ spatial distribution. *Paw U* [1991] also stressed the importance of azimuthal anisotropy. Thus, we define two indicators, $\Delta T_{B,AVG}$ and $\Delta T_{B,STD}$ (see notation section), for the following analysis. Herein, 55° is selected to represent the off-nadir brightness temperature based on the geometry of ATSR and MODIS. The crop-air temperature difference ($T_B(\theta) - T_a$) is introduced because it plays a key role in energy budget analysis.

2.5. Impacts of Environmental Parameters

[15] Based on the field measurement on a grass site from June to October, *Chehbouni et al.* [2001b] indicated that grass biomass and soil moisture have great effect on $T_B(\theta)$, which depends implicitly on weather conditions, such as wind speed and incident solar radiation. Therefore, the relationship between $T_B(\theta)$ and the environmental parameters, such as wind speed, solar radiation, air temperature, soil water content, and LAI, etc., are analyzed by changing input values of these variables. Sensitivity is assessed using variations of $\Delta T_{B,AVG}$.

3. Field Sites

[16] Two field sites for winter wheat (Beijing, China) and summer corn (Hebei Province, China) are selected to simulate temporal variations and determine diurnal patterns. The winter wheat site provides 22 days of data for simulation and sensitivity analysis, among them, 2 days of

Table 1. Environmental Data for the Winter Wheat Canopies From DOY 84 to 111 and for Summer Corn Canopies From DOY 205 to 226[a]

Winter Wheat Canopies							Summer Corn Canopies						
DOY	Date	T_a	h_a	u	R_{tot}	w_s	DOY	Date	T_a	h_a	u	R_{tot}	w_s
84	25 Mar	9.0	4.5	1.6	15.11	18	205	24 Jul	22.8	22.3	0.8	18.4	7.3
91	1 Apr	16.3	6.7	1.5	19.01	12.8	206	25 Jul	24.0	24.6	0.8	16.1	8.3
92	2 Apr	13.9	5.8	1.2	18.77	5.0	207	26 Jul	23.5	25.8	0.7	4.3	11.8
93	3 Apr	9.9	4.5	1.7	14.10	4.6	208	27 Jul	23.5	25.2	1.0	14.2	9.4
94	4 Apr	11.2	5.9	1.7	*7.959*	5.1	209	28 Jul	24.4	26.7	0.8	12.1	11.2
95	5 Apr	12.5	5.2	2.6	*16.06*	5.2	210	29 Jul	24.3	26.6	0.9	8.3	11.2
96	6 Apr	9.5	6.2	2.2	*6.67*	22.7	211	30 Jul	24.9	26.8	0.9	14.0	9.4
97	7 Apr	11.0	9.2	1.8	*11.79*	21.0	212	31 Jul	24.6	28.5	3.2	4.9	13.4
98	8 Apr	15.2	11.5	1.9	*9.52*	20.8	213	1 Aug	25.3	25.5	3.2	17.1	8.8
99	9 Apr	9.1	9.5	2.3	*13.75*	22.7	214	2 Aug	25.7	27.3	3.2	11.1	7.9
100	10 Apr	10.4	4.4	3.5	21.04	16.9	215	3 Aug	24.8	26.9	3.2	8.8	9.1
101	11 Apr	12.2	3.7	2.7	20.29	8.6	216	4 Aug	24.1	26.1	3.2	9.4	9.0
102	12 Apr	13.2	4.8	1.7	24.04	14.9	217	5 Aug	24.6	26.6	3.2	12.2	8.7
103	13 Apr	14.4	5.0	3.6	21.97	0.6	218	6 Aug	27.3	25.9	3.2	10.0	8.1
104	14 Apr	17.1	4.2	2.8	19.97	26.2	219	7 Aug	25.9	28.9	3.2	10.2	8.6
105	15 Apr	17.5	5.8	1.6	22.01	17.7	220	8 Aug	24.4	29.1	3.2	2.8	12.3
106	16 Apr	20.5	6.9	1.6	17.64	18.9	221	9 Aug	25.8	22.8	3.2	17.2	7.4
107	17 Apr	19.7	11.2	1.7	15.31	15.1	222	10 Aug	25.5	19.5	3.2	19.8	5.4
108	18 Apr	22.2	15.3	1.5	19.79	18.8	223	11 Aug	25.8	18.9	3.2	18.8	5.2
109	19 Apr	17.0	5.5	4.1	15.61	10.8	224	12 Aug	25.5	14.4	2.9	14.3	5.2
110	20 Apr	11.1	6.0	1.2	20.43	18.8	225	13 Aug	26.1	21.6	3.3	24.4	5.3
111	21 Apr	13.4	6.6	1.4	15.11	20.8	226	14 Aug	26.8	21.6	3.3	22.3	7.8

[a]Daily average air temperature T_a (°C), air humidity h_a (mb), wind speed u (m/s), soil surface water content w_s (%), and daily total solar radiation R_{tot} (MJ m^{-2} d^{-1}). Reference heights are 2.0 m and 1.5 m for wheat site and corn site, respectively; LAI is defined from 0.4 to 2.3 at the wheat site and from 0.4 to 1.4 at the corn site. Italic values indicate special low solar radiation.

validation data for dense canopies. The summer corn site provides validation data of 4 days for sparse canopies and 22 days of data for seasonal simulation.

3.1. The Winter Wheat Site

[17] The field experiment over winter wheat canopies was conducted for 22 days, from 1 to 21 April, as well as 25 March 2001, in Beijing (116°34′33″, 40°11′40″), China. The winter wheat was planted in the previous fall. The row orientation was 6° northwest with row spacing of 0.14 m. The average canopy height increased from 0.08 to 0.32 m with LAI from 0.3 to 2.3, as well as the ratio of crop row width/row spacing from 0.3 to 0.7. The mean leaf angle was about 60°. Based on the method from *Kustas and Norman* [1999], clumping index is estimated using LAI and row width data. There was an automatic weather station (AWS) in the field that automatically recorded the micrometeorological data for every half hour at 2 m height from the ground (R_{sun}, T_a, and h_a, u). Soil water content was measured periodically with a neutron probe at depths of 5, 10, 20, 40, 60, and 100 cm. Table 1 shows the daily averages of environmental parameters. Herein, w_s denotes water volume content of soil surface from 0 to 5 cm depth. The soil type was Aquic Brown Soil (a type of salty loam in China) with bulk density of 1.3 g/cm^3 at surface. Field moisture capacity and wilting coefficient were 22% and 10% at the soil surface, respectively. There was a rainfall (about 2–3 cm) on 5 April, and it was irrigated (about 0.6 cm) on 14 April.

[18] Field data on 20 and 21 April 2001 are used to evaluate simulation results. The canopy height was 0.32 m with LAI of 2.3. Row width was about 0.1 m (70% of the row spacing). During these 2 days, atmosphere visibility was 12 km, and daily averaged wind speed was 1.2 m/s. T_a was between 21°C and 4°C.

3.2. The Summer Corn Site

[19] The field experiment over summer corn canopies was conducted in 4 days, including 26 July and 3, 5, and 7 August 2009, in Hebei Province (40°20′56″N, 115°47′03″E), China. The row structure was oriented at east-west. The row spacing was 50 cm, and plant density was 6.7 plants/m^2. LAI varied from 0.5 to 0.9 and mean leaf angle was 45°. The canopy height varied from 1.0 to 1.2 m. The solar short-wave radiation, wind speed, air temperature, and humidity parameters at 1.5 m were acquired hourly from an AWS 10 m away. The soil type was sandy loam soil with surface bulk density of 1.7 g/cm^3. Soil water content was measured periodically with TDR (Time domain Reflectometry) rods at depths of 5, 10, 20, 40, and 50 cm. The surface volume water content was 2%–6%, and moisture at the depth of 50 cm was 15%–23%. During these days, there were frequent thin clouds.

4. Experimental Setup and Data Preprocessing

4.1. Experiment at the Winter Wheat Site

[20] The four-component (sunlit and shaded leaf or soil) temperatures were measured using a thermocouple thermometer (JM424 digital thermometer, thermocouple size of 0.6 mm). The sensor of the JM424 digital thermometer was a K-type thermocouple (contact type) and had a nominal sensitivity of 0.1 K. The thermocouples were placed manually on the surfaces of the soil or leaf for 1 s for each measurement. Sunlit leaf was selected as those fully lit by the Sun. For each component, 12 samples were obtained and

Table 2. Specific Conditions to Test TRGM

Conditions	Scene	SZA	Leaf Temperature (°C)	Soil Temperature (°C)
a	homogeneous; height 0.1 m (LAI = 0.05; LAD = uniform)	90°	30	20
b		10°	20 ± 5	50 ± 10
c	homogeneous; height 2.0 m (LAI = 5.0; leaf angle = 0°)	90°	30	20
d		10°	20 ± 5	50 ± 10
e	row structure; height 2.0 m (LAI = 5.0; leaf angle = 90°)	90°	30	20
f		10°	20 ± 5	50 ± 10

averaged. The emissivities of leaf and soil were measured with a FTIR spectral radiometer (BOMEM 304), which were 0.98 and 0.95, respectively [*Xiao et al.*, 2003]. A two-channel thermal radiometer system (with FOV of 8.4°) was employed to measure $T_B(\theta)$ within the spectra of 8–11 μm and 10.6–14 μm. According to the blackbody calibration data, the thermal radiator had accuracy about 0.3 K. Output signal was recorded every 0.6 s. When mounted on a goniometry system, the TIR radiometer can measure $T_B(\theta)$ by rotating the arm to change the observing zenith angle, and by moving along the track of the goniometer to adjust the azimuth angle. The goniometry system has been used by *Chen et al.* [2002], *Yan et al.* [2003], and *Li et al.* [2004].

[21] The TIR radiometer was mounted on the goniometer arm at 1.8 m above the canopy top. All observations in one profile had the same view azimuth angle whereas the view zenith angle varied from −65° to 65°. The azimuth angle step was set to be 30° and it took about 20 min to complete one set of directional observations, during which the component temperature would change slightly. A correction method was applied to remove the temporal effect adapted from *Liu et al.* [2001]. That is, the mean $T_B(0)$ was first calculated from all profiles. Second, the differences ΔT_{adj} between the mean $T_B(0)$ and $T_B(0)$ of each profile were derived. Then, ΔT_{adj} was added to $T_B(\theta)$ of each profile (equation (1)).

$$T_B(\theta) = T_B(\theta)\left(1 + \frac{\Delta T_{adj}}{T_B(0)}\right). \quad (1)$$

[22] Another thermal radiometer (Konica Minolta, sensitivity of 0.1 K, FOV of 8°) was mounted at 2 m above ground to automatically record off-nadir $T_B(45)$ every 10 min within the spectrum of 8–14 μm. The measured brightness temperatures from 13 to 21 April 2001 were calibrated and used for validation.

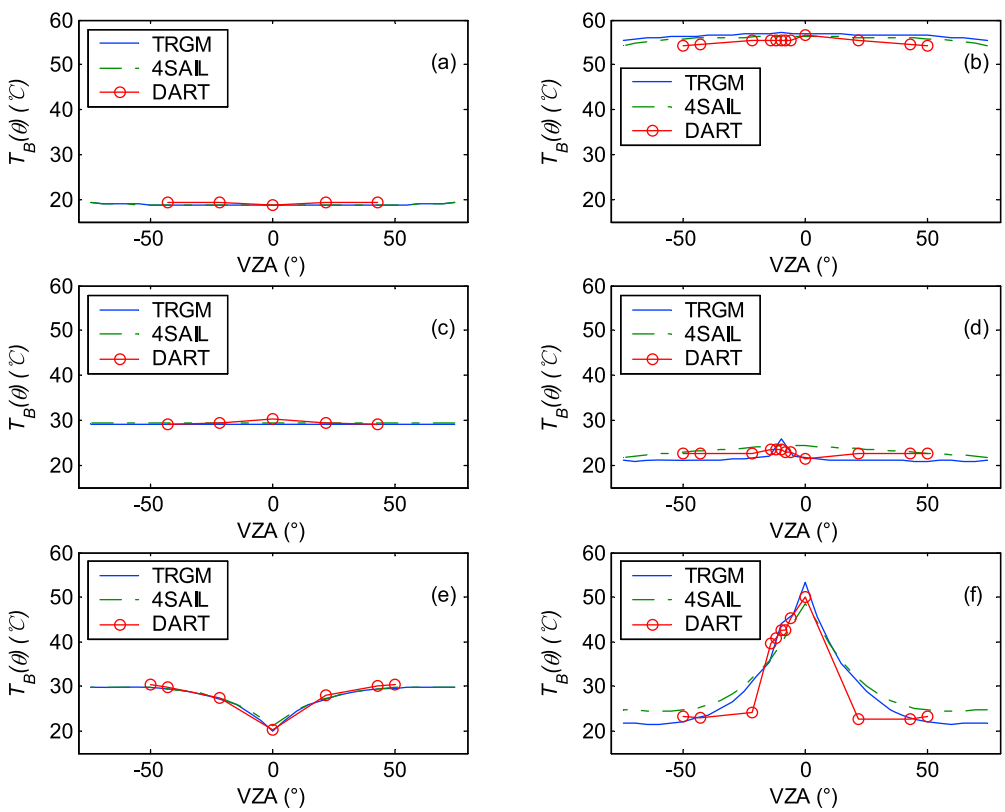

Figure 2. (a–f) Comparisons of $T_B(\theta)$ simulations in solar principal plane for TRGM, 4SAIL model, and DART model corresponding to cases a–f in Table 2.

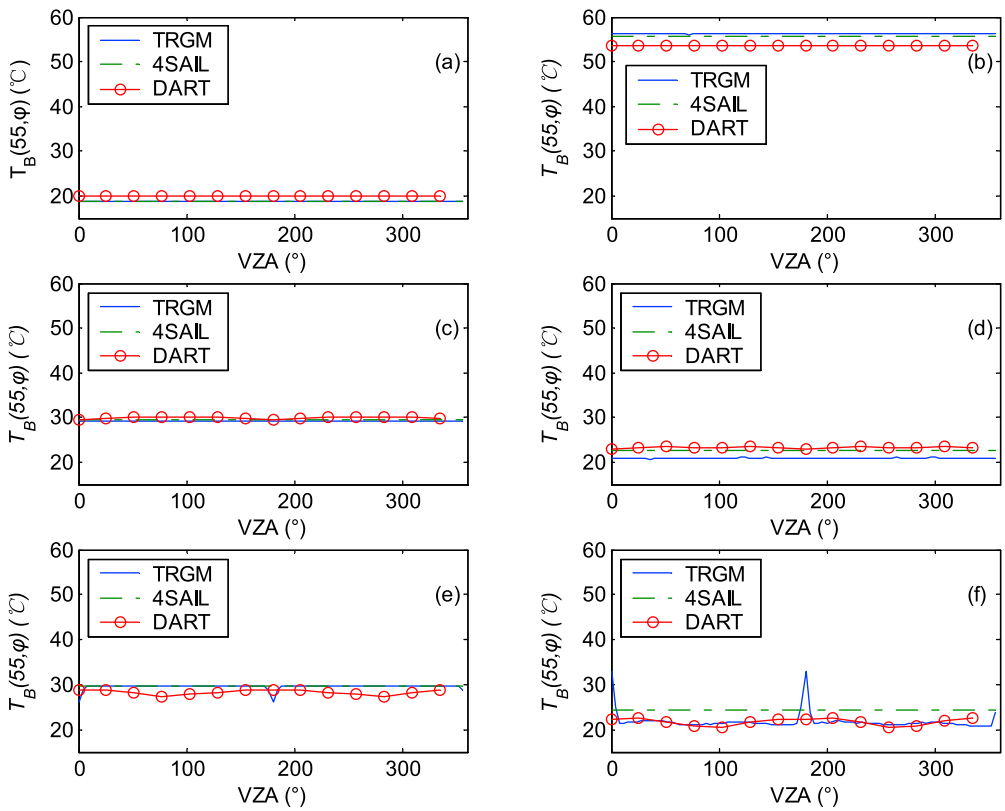

Figure 3. (a–f) Comparisons of $T_B(55, \varphi)$ simulations at azimuth angle from 0° to 360° for TRGM, 4SAIL model, and DART model corresponding to cases a–f in Table 2.

4.2. Experiment at the Summer Corn Site

[23] The four-component (sunlit and shaded leaf or soil) brightness temperatures were measured using an infrared thermometer (AGA Thermopoint 80, sensitivity of 0.1 K) and were then corrected as four-component temperatures using the method from *Liu et al.* [2007]. Sunlit leaf was selected as those fully lit by the Sun. For each component, 12 samples were obtained and averaged. The emissivities of the leaf and soil were set as the default at 0.98 and 0.95, respectively. The directional thermal images were stored in the thermal camera (FLIR S60) with a spectral window from 7.5 to 13.5 μm. The camera was equipped with wide lens that had a field of view (FOV) of 80°. The camera was mounted on a goniometer system and the arm was first rotated from 60° to nadir in the SPP with a step of 5°, and then rotated at four azimuth angles (in SPP and CPP) with a fixed zenith angle of 55°. The goniometer base was at the same height as the top canopy. The arm had a length of 1.6 m. The footprint covered at least two rows; it could also represent the whole field area. Every 1.5 h, data were measured within five minutes.

[24] Three steps were adopted to process the directional thermal images. First, the same method by *Lagouarde et al.* [2000] was used to correct the geometric distortions of the thermal images due to wide-angle lens. Then, a virtual circle method [*Huang et al.*, 2007] was used to derive the directional brightness temperature $T_B(\theta)$ with an equivalent FOV of 20°. The temporal correction method above was also used here. Finally, the $\Delta T_{B,AVG}$ and $\Delta T_{B,STD}$ were estimated using the finite number of $T_B(\theta)$.

4.3. Simulation Data Set

[25] Simulation data set consists of a basic set and sensitivity analysis set. The basic set uses the measured data in 22 days (1–22 April 2001) at the winter wheat site and 22 days (25 July to 15 August 2009) at the summer corn site completely as input and generates the corresponding $T_B(\theta)$ distribution. All the basic sets consist of (1) virtual three-dimensional canopies (rowing on a daily basis), (2) hourly or half-hourly microclimatic parameters (e.g., air temperature, humidity, solar radiation, wind speed, and rainfall), (3) hourly or half-hourly component temperatures (sunlit and shaded soil temperature, leaf temperature profiles in canopies), and (4) hourly or half-hourly $T_B(\theta)$ distributions and derived $\Delta T_{B,AVG}$ and $\Delta T_{B,STD}$.

[26] The sensitivity analysis data set is an extension of the basic set. By changing the input values of wind speed, solar radiation, air temperature, and humidity, soil water content, and LAI to all possible values within their physical ranges, the corresponding variations of $T_B(\theta)$ were determined.

5. Performance of TRGM Under Extreme Conditions

[27] To examine the effect on radiative temperatures as a function of angle, simulations should be conducted first by

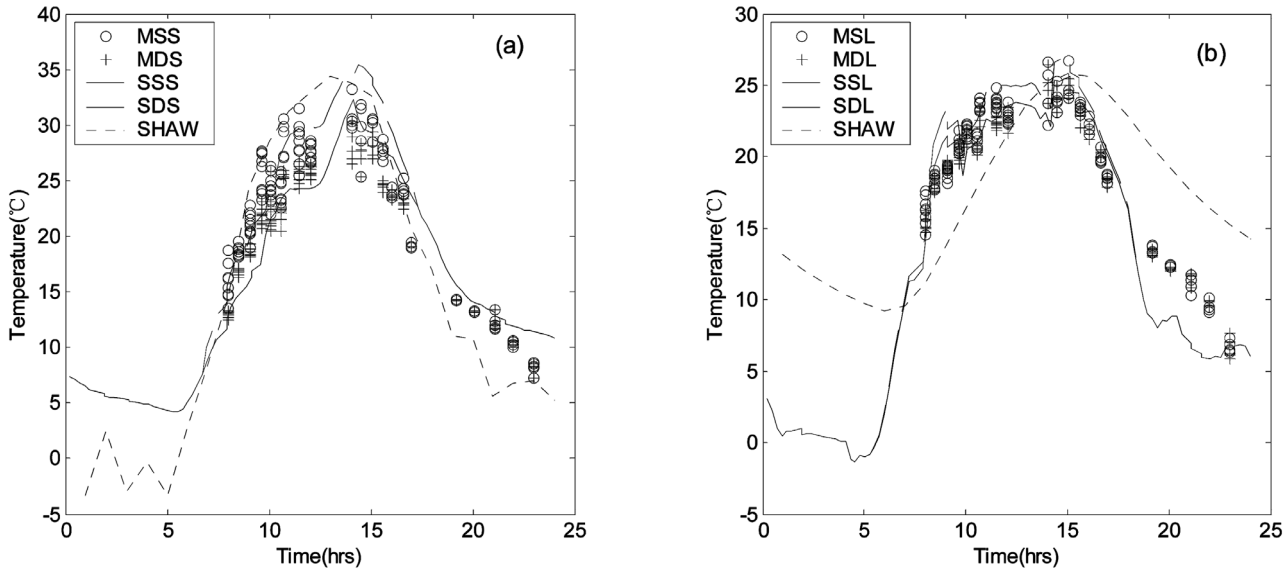

Figure 4. Comparisons between measured (circles and crosses) and simulated (lines) (a) soil temperature and (b) leaf temperature on 21 April 2001. SDS and SDL are the simulated shaded soil and leaf temperature, SSS and SSL are the simulated sunlit soil and leaf temperature, MDS and MDL are the measured shaded soil and leaf temperature, MSS and MSL are the measured sunlit soil and leaf temperature, and SHAW is the simulation result using a multilayer SVAT model–SHAW [*Flerchinger et al.*, 1998].

radiative transfer models using specific input soil and leaf temperature distributions without an actual energy budget.

[28] *Liu et al.* [2007] had already tested the directional variations by TRGM and provided a general picture under normal conditions. However, it is still of great interest to verify TRGM's ability to simulate extreme cases that might occur during daily or seasonal simulations. We focus on component temperature distribution factor under specific extreme conditions (Table 2). These conditions include extreme LAI (0.05 versus 5.0), extreme canopy height (0.1 m versus 2.0 m), extreme leaf angles (0° versus 90°) and extreme solar zenith angle (10° versus 90°) for typical extreme component temperature distributions. The LAI at 0.05 represents very sparse crop canopies (cases a and b in Table 2), whereas 5.0 represents very dense canopies (cases c–f in Table 2). The leaf angle at 90° represents canopies with fully vertical leaves; whereas 0° represents canopies with fully horizontal leaves. Row structure (cases e and f in Table 2) and homogeneous canopies (cases a–d in Table 2) are also compared. The SZA at 90° represents conditions at night or on a cloudy day, whereas 10° represents conditions at noon. The default emissivities of 0.98 and 0.95 for leaf and soil are used.

[29] The simulated $T_B(\theta)$ in SPP and $T_B(55)$ from azimuth angle 0° to 360° are shown in Figures 2 and 3, respectively. Based on the same cases, two radiative transfer models, a homogeneous model 4SAIL [*Verhoef et al.*, 2007] and a heterogeneous model DART [*Guillevic et al.*, 2003] have been used to simulate $T_B(\theta)$ to compare with the results of TRGM. Though for 1-D canopy, 4SAIL accommodates temperatures for a maximum of four components: sunlit leaves, shaded leaves, sunlit soil and shaded soil. DART (Discrete Anisotropic Radiative Transfer) simulates TIR radiative transfer in vegetation landscapes based on 3-D scenes that are discretized as matrices of rectangular cells containing trees, shrubs, grass, and soil. In SPP, the simulated $T_B(\theta)$ trend by TRGM is similar to those by 4SAIL and DART. However, for Figures 2d, 2f, 3d, and 3f, there are significant differences among TRGM, 4SAIL and DART. For homogenous canopies, the simulated azimuth effects are almost the same. For the row structured canopies, only TRGM clearly shows the local variations along/across row direction, which indicates TRGM is feasible and most suitable to simulate both zenith and azimuth effects for row-structured crop canopies. Considering row structure, DART gives closer results to TRGM than 4SAIL.

[30] Based on the performance simulations, the temporal variations of the directional brightness temperature can be simulated by TRGM more accurately than other models with actual energy budget, which will be done by the Cupid model using specific input data from two field sites.

6. Evaluation of the Linked Model

[31] Based on the field measurements, the linked model can be evaluated from the following three aspects. Moreover, to identify the advantage/limitation of the linked model, comparisons with older models are necessary. As mentioned in section 1, among the few old radiative transfer/soil-vegetation-atmosphere models, most methods are designed for homogeneous crop canopies. Therefore, we combine a multilayer SVAT model–SHAW [*Flerchinger et al.*, 1998] and a radiative transfer model–4SAIL [*Verhoef et al.*, 2007] to represent the old models and compare with our two-model method, using the same parameters as far as possible. The Cupid model alone is also used for comparisons of directional brightness temperatures.

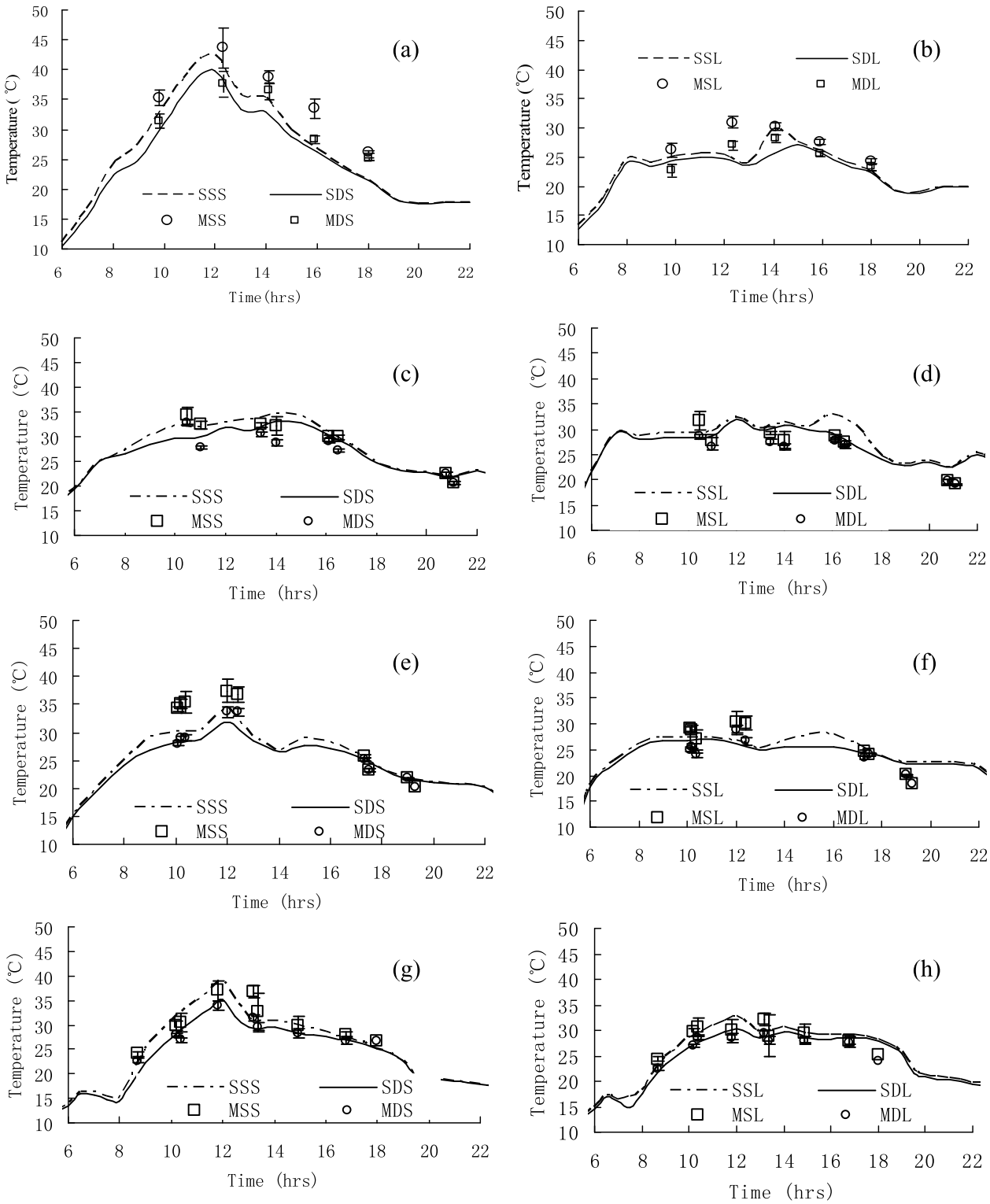

Figure 5. Comparisons between measured (circles and squares) and simulated (lines) (a, c, e, and g) soil temperature and (b, d, f, and h) leaf temperature on 26 July 2009 (Figures 5a and 5b), 3 August 2009 (Figures 5c and 5d), 5 August 2009 (Figures 5e and 5f), and 7 August 2009 (Figures 5g and 5h). SDS and SDL are the simulated shaded soil and leaf temperature, SSS and SSL are the simulated sunlit soil and leaf temperature, MDS and MDL are the measured shaded soil and leaf temperature, and MSS and MSL are the measured sunlit soil and leaf temperature.

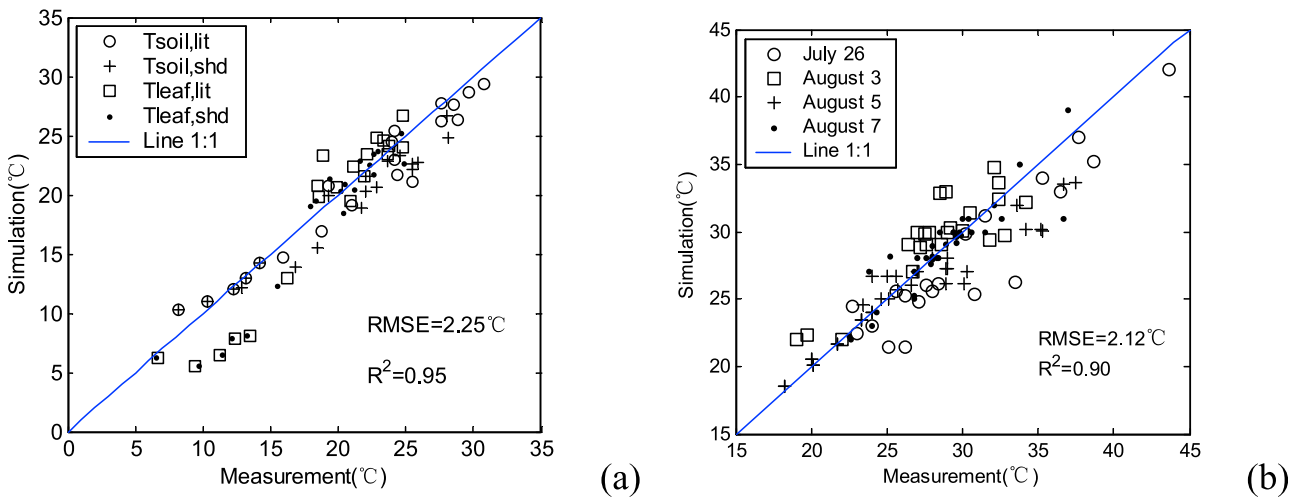

Figure 6. The relationship of all measured component temperatures and simulations: (a) the winter wheat canopy on 21 April 2001 and (b) corn canopies on 4 days in 2009.

6.1. Diurnal Variations of Component Temperatures: Measurement Versus Simulation

[32] Figure 4 shows the simulated and measured component temperatures at the winter site on 21 April 2001. The simulated sunlit and shaded soil temperatures by Cupid are higher than the ones measured in the morning and lower than the ones measured in the afternoon (Figure 4a). For leaf temperatures (Figure 4b), the ones measured are mostly between simulated sunlit and shaded temperature by Cupid during daylight. However, the simulated temperatures are a little lower (about 1°C–3°C) than measured ones after sunset. The SHAW model produces comparable mean soil temperatures but poor mean leaf temperatures with large error up to 10°C. Figure 5 shows the comparisons at the summer corn site from 26 July 2009 to 7 August 2009. Both simulations of leaf and soil temperatures provided similar trend with the measurements. The simulated soil temperatures are underestimated (Figures 5a, 5e, and 5g), as they could rise to 5°C. The leaf temperatures are better simulated than soil temperatures. The larger error on 3 and 5 August can be attributed to the frequent cloud cover.

[33] The correlation coefficients between simulation and measurement of component temperature are 0.95 for winter wheat canopies and 0.90 for summer corn canopies (Figure 6). The overall error is with RMSE of 2.5°C and 2.1°C for winter wheat and summer corn canopies, respectively. Despite the error, the simulated component temperatures in two sites show good agreement with the measured values and provide reasonable input parameters for $T_B(\theta)$ calculation.

6.2. Comparison Between Measured and Simulated Distribution of $T_B(\theta)$

[34] Comparisons over wheat canopies between measured and simulated $T_B(\theta)$ distributions in channels 8–11 μm are displayed in Figure 7. The results are presented in polar contour plots with the polar angle representing view azimuth and concentric circles corresponding to zenith angles. The north is assumed to be with the azimuth angle of 0°. The gray scale that indicates $T_B(\theta)$ values has been adapted for every plot to make spatial variations more visible. White represents higher $T_B(\theta)$, while black represents lower $T_B(\theta)$. Measurement and simulation have a similar trend, including hot spot position and hot stripe (row structure effect). The $\Delta T_{B,AVG}$ from the measurement was greater than the simulations by all the three models. The maximum difference between the measured and simulated $T_B(\theta)$ is about 3°C in large view zenith angles. That is because the Cupid model predicts higher leaf temperature but lower soil temperature, leading to smaller temperature difference between the soil and leaf. As a result, the $T_B(\theta)$ variations with view zenith angle become smaller. The comparisons at the corn site on 7 August 2009 are presented in Figure 8. The measurements and simulations of $T_B(\theta)$ are consistent but are better matched at the backward direction than that of wheat canopies.

[35] Figure 7f shows the comparisons of azimuthal variations at the wheat site. According to the measurements, the maximum azimuthal difference is up to 4°C with the highest $T_B(55)$ at the backward direction and the lowest $T_B(55)$ at cross-row directions. All the three models significantly underestimated the azimuthal variation (<1°C). Because SHAW can only simulate a mean temperature per layer and 4SAIL cannot consider row structure, the SHAW-4SAIL model did not show any azimuthal variation. The underestimation of Cupid alone or the coupled model was due to the underpredicted temperature difference between the soil and leaf by the Cupid model. As to the variation trend, the Cupid model alone showed variation around SPP, but not around cross-row directions. Considering the variations around the cross-row directions, the coupled model shows closer trend with the measurements. Due to the four limited azimuth observations, the azimuthal variation at the corn site is not presented here.

[36] Generally, the simulated $\Delta T_{B,AVG}$ by the coupled model is lower (1°C–2°C) than the measurement. However, the evaluation demonstrates that the two linked models are capable of simulating the directional effect trend varying with time and view angle.

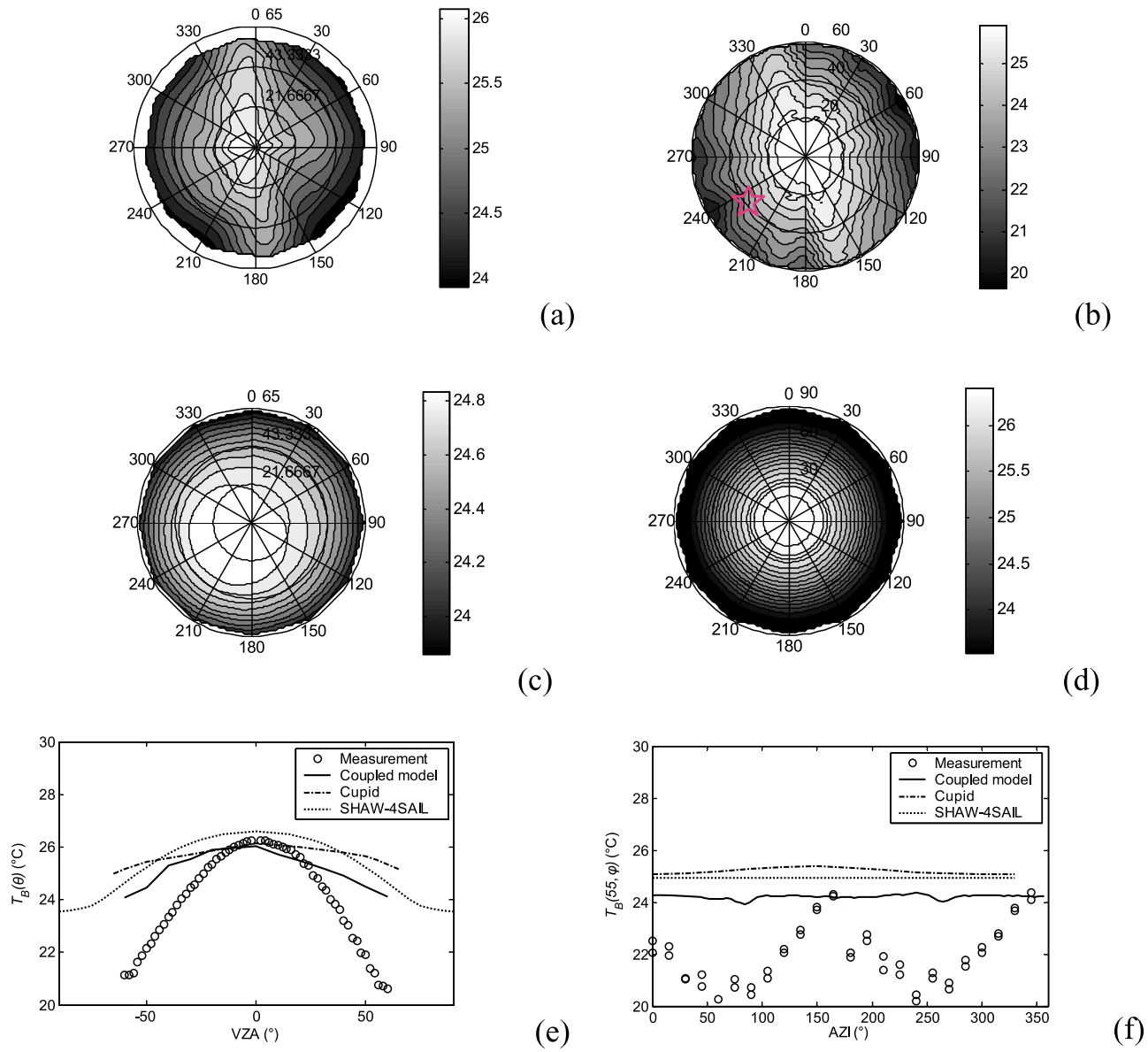

Figure 7. Comparisons of the (a) two-model-simulated $T_B(\theta)$, (b) measured $T_B(\theta)$, (c) Cupid simulated $T_B(\theta)$, (d) SHAW-4SAIL simulated $T_B(\theta)$, (e) $T_B(\theta)$ profiles in solar principal plane, and (f) $T_B(55,\varphi)$ profiles from 0° to 360° at 1400 LT on 21 April 2001. The Sun position was at (37.5°, 228.7°), marked as a star in Figure 7b.

6.3. Evaluation of Simulated $T_B - T_a$

[37] In the Cupid model, T_a is an input parameter; therefore, the variations of $T_B - T_a$ with angle are the same with the angular variations of $T_B(\theta)$, indicating that $\Delta T_{B,AVG}$ and $\Delta T_{B,STD}$ can represent the directional effect of $T_B - T_a$. Herein, only results of temporal variation at a single direction, nadir or off nadir, are shown.

[38] Figures 9a and 9b show the comparisons of crop-air temperature difference ($T_B(0) - T_a$) between measurements and simulations in the winter wheat site on 21 April 2001 and the summer corn site on 7 August 2009. Because the SHAW model produced poor soil or leaf temperatures, the SHAW-4SAIL model highly overestimates the $T_B(0) - T_a$. Both the coupled model and Cupid showed similar trend with the measurement ($R^2 > 0.90$). However, absolute accuracy was rather lower for the summer corn canopy (RMSE = 4.7°C) and could be due to the influence of frequent thin clouds. The hourly weather station measurements were insufficient to record the instant solar radiation variations during measurements. Figure 9c shows a continuous comparisons of off-nadir crop-air temperature difference ($T_B(45) - T_a$) between measurements and simulations in the winter wheat site from 13 to 21 April 2001. The azimuth angle was east (90°). The coupled model showed better agreement ($R^2 = 0.91$, RMSE = 2.4°C) with measurement than the Cupid model ($R^2 = 0.87$, RMSE = 2.8°C).

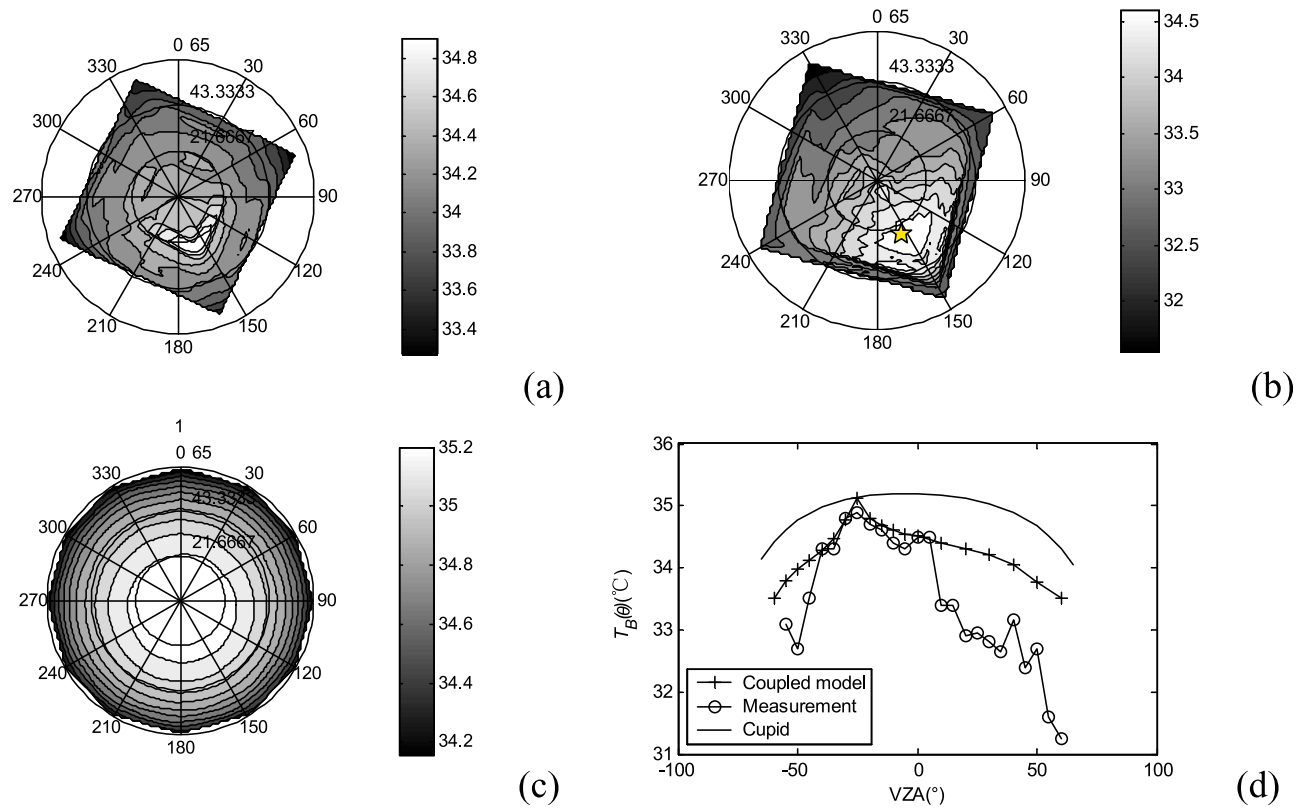

Figure 8. Comparisons of the (a) two-model-simulated $T_B(\theta)$, (b) measured $T_B(\theta)$, (c) Cupid simulated $T_B(\theta)$, and (d) $T_B(\theta)$ profiles in solar principal plane at midday on 7 August 2009. The Sun position was at (26°, 156°), marked as a star in Figure 8b.

[39] Note that DART was not compared here because its energy balance (EB) module of component temperature simulation has not yet completed (or not available online). Having been compared without energy balance in section 5, it is not necessary to run DART again by using the input of component temperatures from SHAW or Cupid.

7. Results

7.1. Simulated Temporal Pattern of Directional Brightness Temperature

[40] Figure 10 shows the simulated diurnal variations of $\Delta T_{B,AVG}$ and $\Delta T_{B,STD}$ at the wheat site during the 22 days in 2001 based on two-model simulation data sets. In most days, the $\Delta T_{B,AVG}$ behaved in a "W" shape, with the middle peak at midday (1200–1300 LT), and the two valleys in the early morning (0630–0850 LT) or the late afternoon (1745–1910 LT). The two other peaks representing midnight were significantly lower than the middle peak. Herein, $\Delta T_{B,STD}$ has a similar trend except for the absolute value (i.e., about one third of $\Delta T_{B,AVG}$), indicating that the azimuth angular effect should also be considered especially around midday.

[41] The simulated seasonal variations of $\Delta T_{B,AVG}$ and $\Delta T_{B,STD}$ at the wheat site are shown in Figure 10. Strong directional effect can be found in several days, including DOY 93 and DOY 104 with the highest $\Delta T_{B,AVG}$ occurring at midday. On the contrary, there were two periods without significant directional effect, including the days between DOY 94 and 99, and days after DOY 105. These variations are mainly correlated with soil surface moisture (w_s) (Figure 11). The maximum $\Delta T_{B,AVG}$ are up to 2.8 K on DOY 93 with w_s of 5%.

[42] Figure 12 shows the simulated diurnal variations of $\Delta T_{B,AVG}$ and $\Delta T_{B,STD}$ at the corn site from 26 July to 10 August 2009. The "W" shape of $\Delta T_{B,AVG}$ appeared again with similar features of wheat canopies.

7.2. Observed Evidence of Temporal Variations of Directional Brightness Temperature

[43] The diurnal variations of $\Delta T_{B,AVG}$ and $\Delta T_{B,STD}$ observed at the wheat site on 20 and 21 April 2001 are shown in Figure 13. The 4 days of observations at the corn site are shown in Figure 14. Both full cover wheat canopies and sparse corn canopies showed similar diurnal patterns of $\Delta T_{B,AVG}$ with a peak at midday and a valley at late afternoon. At the wheat site, the $\Delta T_{B,STD}$ is about from one fifth to one third of $\Delta T_{B,AVG}$. At the corn site, the $\Delta T_{B,STD}$ is more than one half of $\Delta T_{B,AVG}$. Only four $T_B(55)$ in SPP and CPP is available and used to calculate the $\Delta T_{B,STD}$; hence, the azimuth variation at corn site is less credible. However, the comparable $\Delta T_{B,STD}$ with $\Delta T_{B,AVG}$ demonstrates the importance of azimuth variations in sparse canopies. Compared with the simulated $\Delta T_{B,AVG}$, the measurements are 2.0°C higher on 20 April; 1.5°C higher on 21 April; 1.4°C

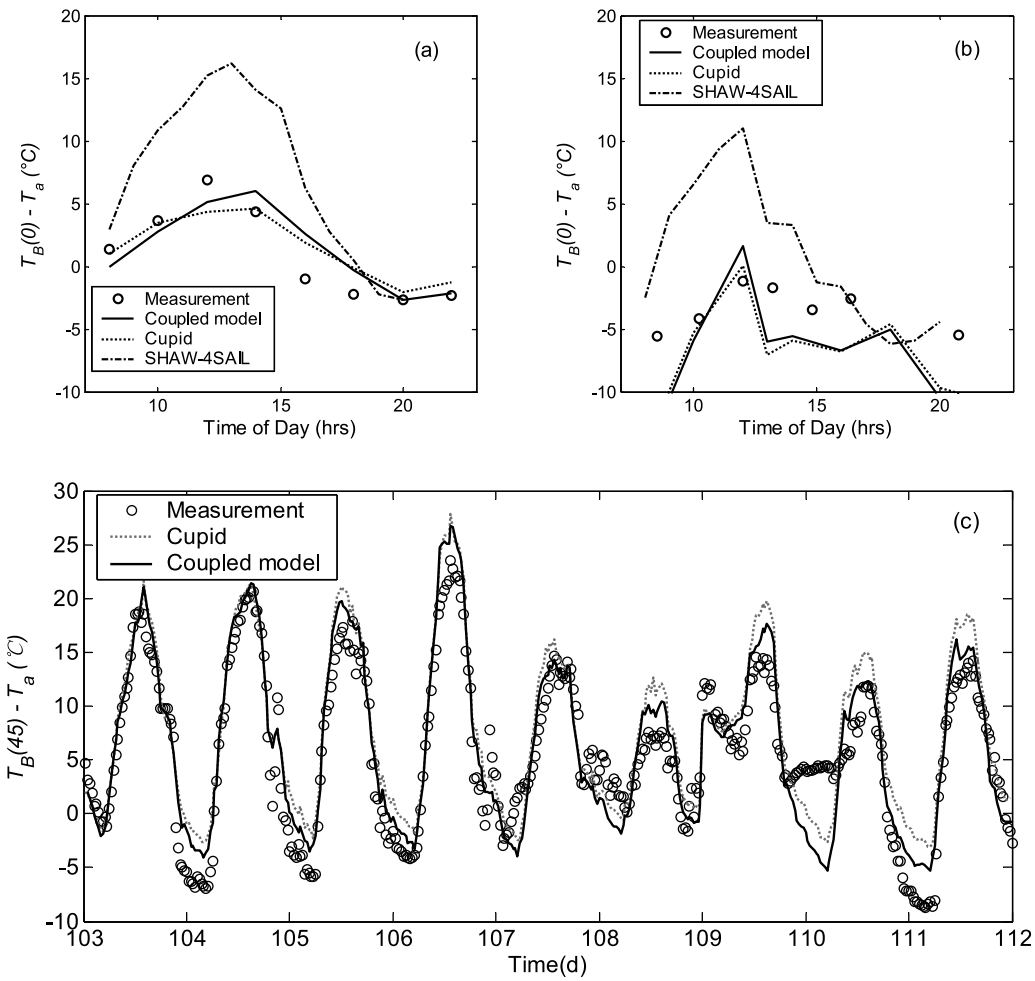

Figure 9. Measured and simulated directional brightness temperature $T_B - T_a$: (a) $T_B(0) - T_a$ of the wheat canopy on 21 April 2001, $R^2 \approx 0.96$, RMSE ≈ 1.8°C; (b) $T_B(0) - T_a$ of the corn canopy on 7 August 2009, $R^2 \approx 0.91$, RMSE ≈ 4.7°C; and (c) $T_B(45) - T_a$ of wheat canopies from 13 to 21 April 2001, $R^2 \approx 0.91$, RMSE≈2.4°C. Error calculations were not done for SHAW-SAIL results due to the large bias.

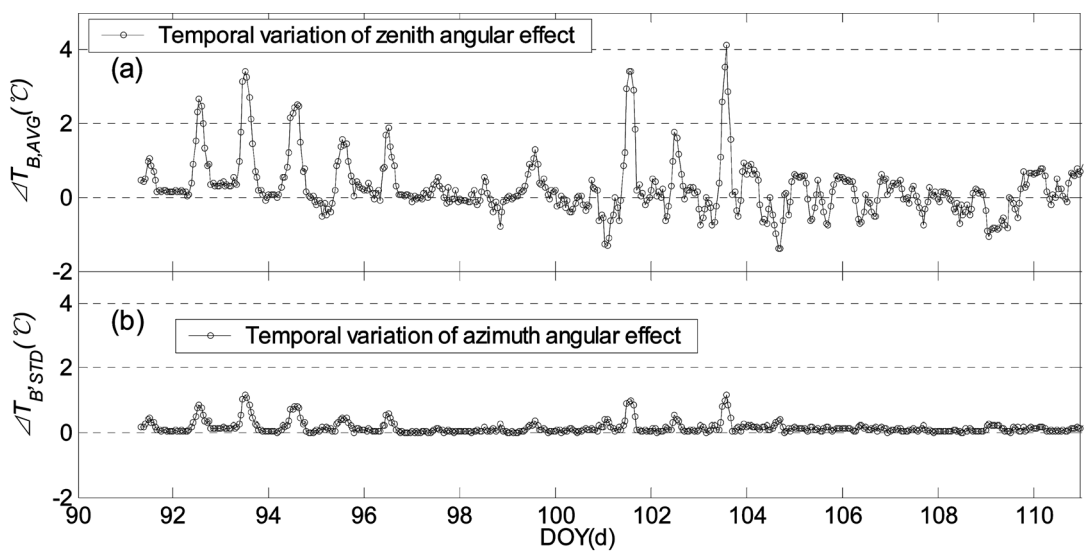

Figure 10. Temporal variations of (a) $\Delta T_{B,AVG}$ and (b) $\Delta T_{B,STD}$ for the wheat canopies from 1 to 21 April.

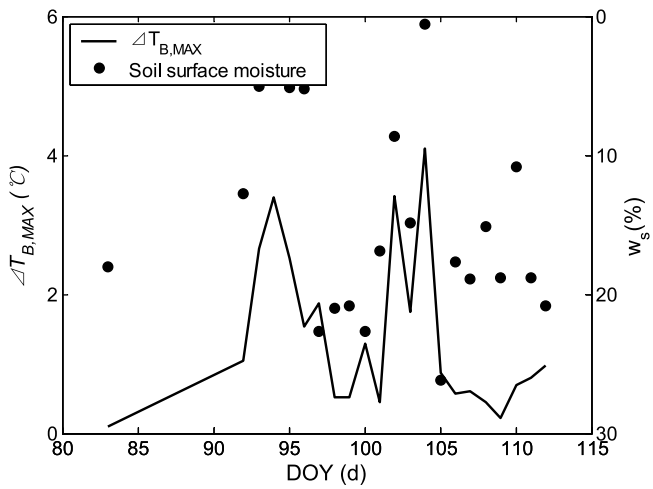

Figure 11. Seasonal variations of $\Delta T_{B,AVG}$ (midday, $\Delta T_{B,AVG}$) correlated with soil surface moisture (w_s, R^2 = 0.69, RMSE = 0.64°C) for the wheat canopies from DOY 84 to 111.

higher on 26 July; 0.3°C higher on 3 August; 0.3°C higher on 5 August; and 0.7°C higher on 7 August.

7.3. Factors Affecting Directional Effect

[44] Based on simulation data, there are five sensitive parameters that affect the $\Delta T_{B,AVG}$, including w_s, T_a, LAI, R_{sun}, and u. Among these parameters, w_s, R_{sun}, and LAI affect $\Delta T_{B,AVG}$ more steadily. Taking 1030 LT on 17 April 2001 as an example, Figure 15 is presented to show the following results.

[45] First, w_s has the most dramatic effect on $\Delta T_{B,AVG}$, increasing by over 2°C as soil became extremely dry.

[46] Second, the effect of LAI peaks at around 0.8, and then decreases as LAI increased. This is an interesting addition to Chehbouni's conclusion [*Chehbouni et al.*, 2001b] that vegetation biomass is a significant factor affecting $T_B(\theta)$ distributions.

[47] Third, the effect of R_{sun} increases nearly linearly as the R_{sun} increases at a rate of about 0.09°C per 100 W m^{-2}.

[48] A higher T_a will decrease $\Delta T_{B,AVG}$ at the wheat site, but will increase $\Delta T_{B,AVG}$ at the corn site. When u is greater than 2 m/s, large wind speeds mostly decrease $\Delta T_{B,AVG}$. Otherwise, increasing wind speed can slightly increase $\Delta T_{B,AVG}$. Results indicate that the effects of air temperature and wind speed are not clear and are relatively lower than those of w_s, LAI and R_{sun}.

[49] Further analysis shows that there is also a strong relationship between soil net radiation, LAI, and $\Delta T_{B,AVG}$ (Figure 16). $\Delta T_{B,AVG}$ and LAI can be derived from satellite data; thus, the soil net radiation can be estimated from $\Delta T_{B,AVG}$ and LAI. To evaluate the relationship, observed soil surface net radiation is calculated using the method from *Kustas and Norman* [1999] based on measured total net radiation at the wheat site and from *Sánchez et al.* [2008] based on total radiation, component temperatures, and downward sky radiation at the corn site. Figure 17 shows through simulation (Figure 16) that the relationship does exist in both sites. The fitted relationship (equation (2)) is slightly affected by the row structure and extinct coefficient (κ, usually 0.6–1.0) of crop canopies. The κ is set to 0.65 for wheat canopies and 0.82 for corn canopies according to the leaf angle distribution (LAD). The correlation of observation cases is significantly lower than the simulated cases (Figure 16). Main errors come from the corn site, including a first-order estimation of soil net radiation under 2 days with thin cloud. If the net radiation was measured directly, we believe the correlation will be better.

$$\Delta T_{B,AVG} = 0.006 R_{n,soil} \exp(\kappa \times LAI) + 0.5. \quad (2)$$

[50] In fact, the product of $R_{n,soil}$ and exp(κ × LAI) is equal to the total net radiation of the canopy [*Kustas and Norman*, 1999] for first-order estimation. However, simu-

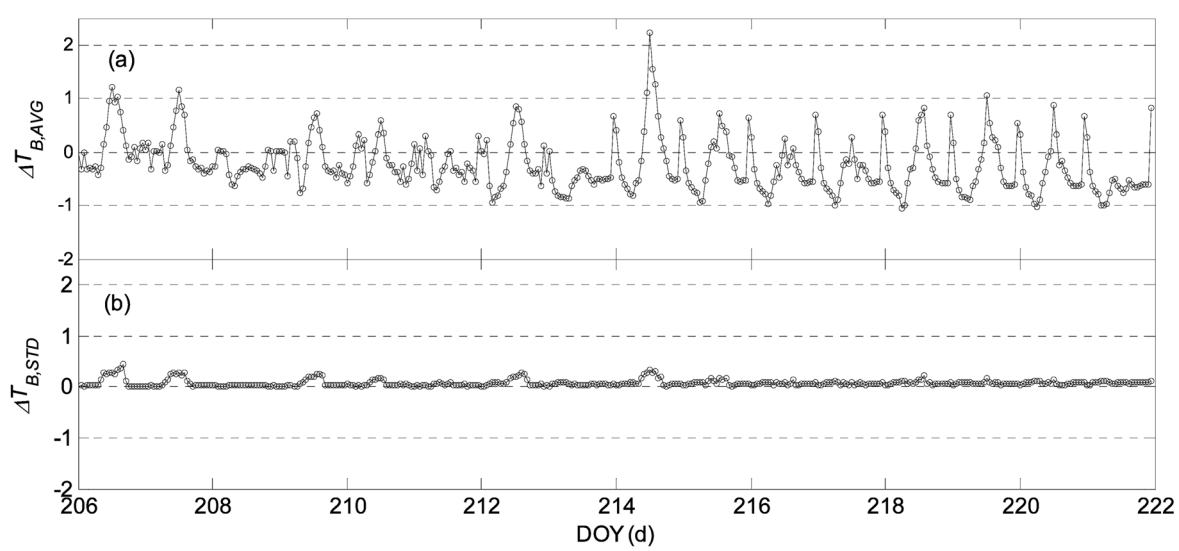

Figure 12. Temporal variations of (a) $\Delta T_{B,AVG}$ and (b) $\Delta T_{B,STD}$ for the corn canopies from 26 July to 10 August. The vertical units are in °C.

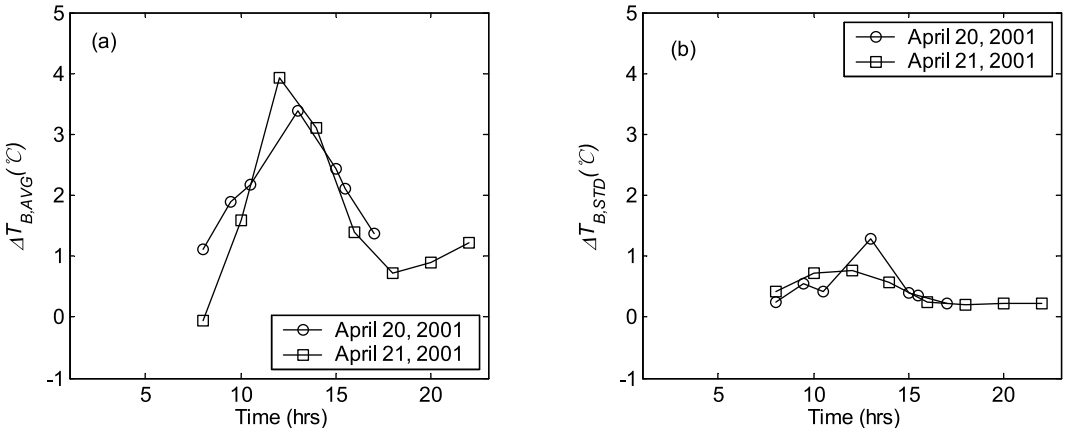

Figure 13. Observed diurnal patterns of directional effect of brightness temperature at the wheat site: (a) $\Delta T_{B,AVG}$ and (b) $\Delta T_{B,STD}$.

lation results of Cupid show that total net radiation is not good in some cases (e.g., after midday on 10 April at wheat site), and the reason why we did not use total net radiation directly.

8. Discussion

8.1. Temporal Patterns of Directional Effect

[51] Simulation and measurement both show diurnal patterns of "W" shape on clear days. This feature can be explained by the formation of $\Delta T_{B,AVG}$. The global shape of directional effect, defined by $\Delta T_{B,AVG}$, is controlled mainly by three factors: (1) the temperature difference between soil and leaf, (2) view proportions of soil or leaf, and (3) emissivities of soil or leaf. Generally, factor 3 is stable and factor 1 is relative small during night. Within the fixed row structure and the LAI and LAD in a given day, factor 2 is stable at any view direction and the temperature difference between soil and leaf plays the most important role on $\Delta T_{B,AVG}$. The θ_s is smallest at midday and the solar direct radiation is the strongest, resulting in the strongest temperature contrast between the soil and leaf. This temperature contrast plays a major role on the maximum $\Delta T_{B,AVG}$. During nighttime, no sunlit components are for both leaf and soil, which results in very close temperature between soil and leaf and hence a low $\Delta T_{B,AVG}$. In the early morning, the top canopy begins to receive more radiation than the soil background, with leaf heating up quickly and the soil remaining cold. At this time period, $\Delta T_{B,AVG}$ becomes even lower than that at night with a high possibility of being negative. After that, soil soon receives solar radiation and heats up quickly, whereas leaf temperature slowly increases because of the physiological control of the leaf. Thus, soil and leaf temperature difference will become increasingly larger until midday. From midday to late afternoon, both soil and leaf temperature may first continue to increase until 1400 LT due to thermal inertia and then decrease. During the period, the temperature difference between soil and leaf continues to decrease until it reaches the lowest value at late afternoon. After late afternoon, both soil and leaf loses direct solar radiation and their temperatures slowly become closer, leading to a slight increase in $\Delta T_{B,AVG}$. Soil water content significantly

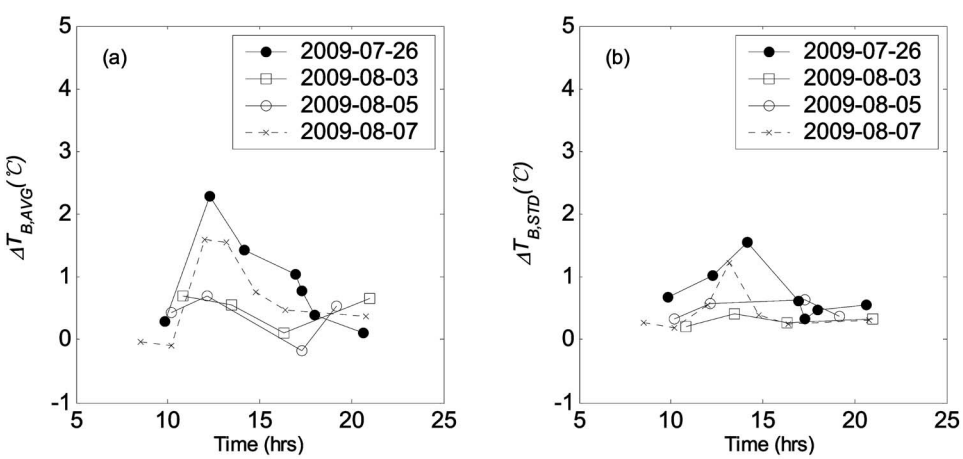

Figure 14. Observed diurnal variations of directional effect of brightness temperature at the corn site: (a) $\Delta T_{B,AVG}$ and (b) $\Delta T_{B,STD}$.

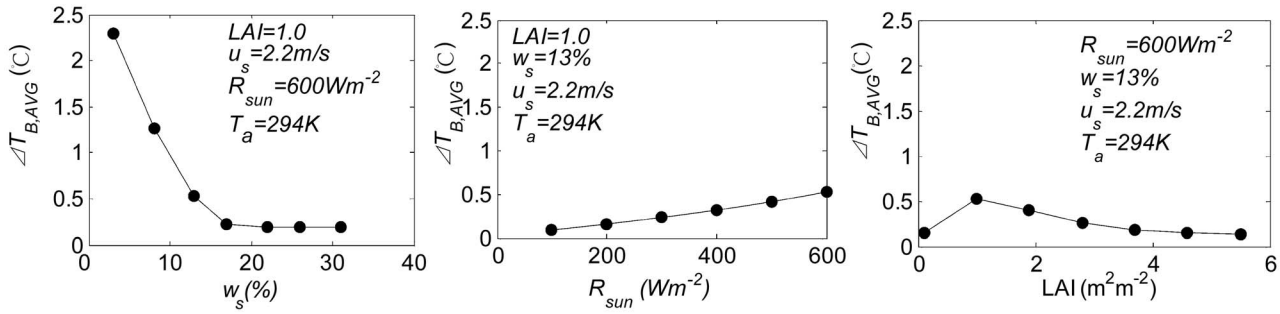

Figure 15. Sensitivity analysis of three major parameters affecting ΔT_B: w_s, R_{sun}, and LAI. The other input parameters are the same at 1030 LT on 17 April 2001.

affected soil and leaf temperature difference, thereby affecting $\Delta T_{B,AVG}$.

[52] This "W" shape might explain why *Chehbouni et al.* [2001b] selected directional effect at midday as the indicator for seasonal comparison. In the winter wheat site, the lower $\Delta T_{B,AVG}$ from DOY 94 to DOY 99 is due to the low R_{tot} and high w_s caused by rainfall. The weak effect after DOY 105 can be explained by the dense canopy structure that affected the $T_B(\theta)$ seasonal variations. This effect occurs because the solar radiation was mostly intercepted by the dense vegetation canopy and soil temperature is lower than the leaf temperature. In the summer corn site, constant wind sweep and frequent cloud movement somehow destroyed the "W" pattern. Therefore, the typical "W" pattern occurs only on cloudless day with slow wind speed. Also, the lower the canopy height, the more typical of the "W" shape because the strong turbulence weakens temperature contrast. That is why the results over winter wheat canopies are always better than that of summer corn canopies.

[53] When the temperature of the sunlit soil or leaf was significantly higher than that of shadowed soil or leaf, a local variations or the so-called thermal "hot spot" effect would occur [*Huang et al.*, 2010]. Azimuthal variations $\Delta T_{B,STD}$ can appear as another local variation, and is small for homogenous canopies but significant for row structure canopies. Different LAD will slightly change $\Delta T_{B,STD.}$

[54] Several curve fitting experiments have shown that a single sinusoid was insufficient to describe diurnal patterns. The combination of three to four sinusoids has the capability to fit the "W" shape, indicating that the diurnal variations of directional effect was more complex than the variations of the soil or leaf temperature alone.

8.2. Potential Application of the Directional Effect

[55] The two-model approach provides some new and promising results for crop canopy emission directionality that could be helpful in understanding the TIR emission directionality mechanism. For example, the results provide a possible way to invert soil net radiation using remote sensing data with multiple view angles (e.g., ATSR). Another application is to normalize the brightness temperature to a single view angle for mapping comparable and accurate surface temperature distribution in an entire image covering a large area (e.g., MODIS). A user can also choose the best time and view angles from the thermal images based on the temporal patterns of $\Delta T_{B,AVG}$. In section 6.3, crop-air

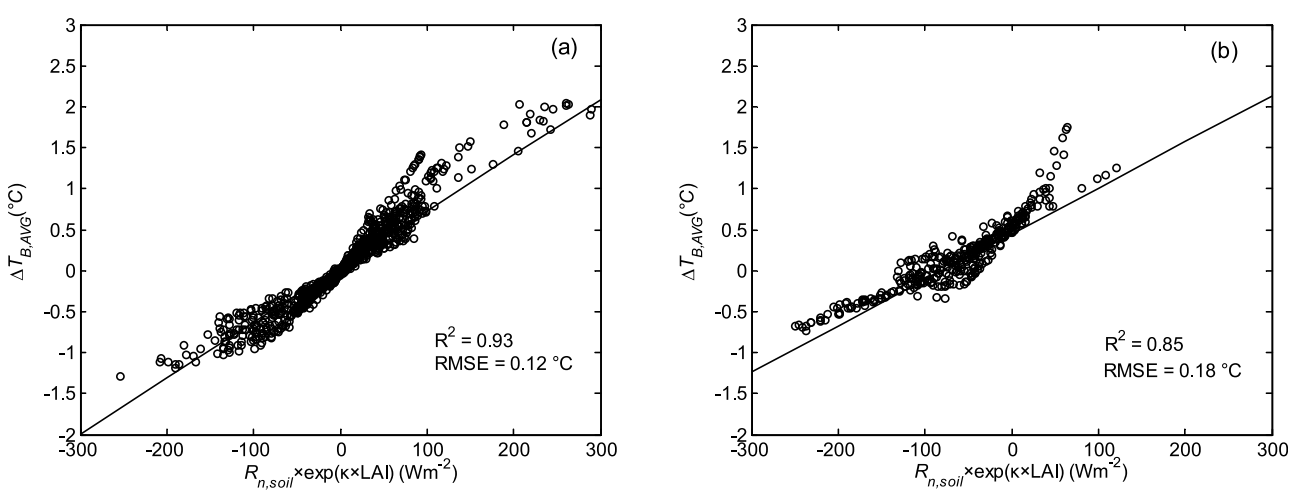

Figure 16. The relationship between $\Delta T_{B,AVG}$ and soil surface net radiation $R_{n,soil}$: (a) wheat canopies from 1 to 22 April 2001 and (b) corn canopies from 26 July to 10 August 2009. The horizontal axis represents the product of soil net radiation and exponential value of leaf area index.

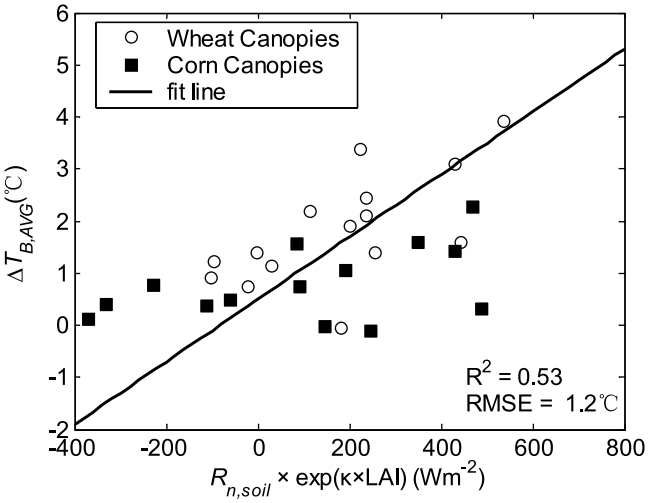

Figure 17. Observed relationship between $\Delta T_{B,AVG}$, LAI, and the soil net radiation $R_{n,soil}$. The horizontal axis represents the product of soil net radiation and exponential value of leaf area index.

temperature difference ($T_B - T_a$) was reasonably simulated by the linked model. Surface-air temperature difference is usually used for energy budget analysis; hence, directional effect could be utilized further.

8.3. Limitations of the Analysis

[56] In this paper, significant temporal pattern of directional effect has been found using the two-model simulation. Simple combined 1-D models, such as SHAW-4SAIL, cannot simulate azimuthal variation and may overestimate the directional brightness temperatures with large error up to 10°C. Cell-based 3-D models, such as DART, are more used for forest/urban landscape than for crop canopies (very few papers were found). One possible explanation is that the cell size needs to be comparable to the row width. If each cell contains statistically enough crop elements, and the benefit of spatial heterogeneity defined by cell matrix somehow loses. To our knowledge, the coupling method and corresponding results are new and useful for energy balance research. However, there are still several limitations to the analysis.

[57] First, the coupling simulation is driven mostly by site-specific input parameters. The temporal pattern might be different and should be used carefully under very different conditions (e.g., different climate zones or other crop types). Simulations should be conducted over a greater number of locations and weather conditions. More field observations are also required.

[58] Second, despite the well-predicted trend of component temperature variations, the Cupid model normally underestimates the differences between soil and leaf temperature that finally lead to lower directional effects than measurements. The negative bias (underestimation) of $\Delta T_{B,AVG}$ by Cupid makes it difficult for us to analyze the quantitative relationships between $\Delta T_{B,AVG}$ and net radiation directly, except for their trend. This error may be due to the iteration algorithm of air temperature/moisture profile used in the Cupid model.

[59] Third, only two indicators are used in this paper to represent the global directional effects. In fact, there are at least two interesting local variations observed, including the hot spot variations and local azimuthal variations normally occurred along or at cross row direction (Figures 3e and 3f). Besides, despite that most hot spot models can correctly predict the peak, the largest differences may be found in near–hot spot angles, depending on accuracy/effectiveness of different hot spot models. The above three local variations are also time related and contain rich information on component temperature distribution and row structure. In our next research, we will focus on them.

[60] Fourth, we are aware that the field scale is different from airborne and satellite scale that would have mixture pixel effect, relief effect or atmospheric effect. Our findings might be adapted before application. This issue needs to be addressed in future studies.

9. Conclusion

[61] By linking the Cupid model that simulates leaf and soil temperature and TRGM that simulates canopy directional brightness temperature $T_B(\theta)$, the temporal patterns of thermal emission directionality were studied in this paper. Two indicators, $\Delta T_{B,AVG}$ and $\Delta T_{B,STD}$, are defined to describe the directional effect. The experimental validation shows that the two-model combination approach gives reasonable, higher temporal resolution results. The general trend is similar to the Apparent Directional Radiation Temperature exported by Cupid; hence, it is clear that the simple models could be adequate for many purposes, particularly for canopies of full cover. However, the Cupid model alone, or combined 1-D models like SHAW-4SAIL, cannot simulate substantial variations of $\Delta T_{B,STD}$ for typical row structure canopies or sparse discrete canopies. Even for full cover canopies, the directional effect would be somehow underestimated by Cupid. Thus, a better result was achieved by considering the 3-D canopy structure, especially the row structure effect.

[62] Significant diurnal and seasonal variations of $\Delta T_{B,AVG}$ are also found. In most days, the $\Delta T_{B,AVG}$ behaves like a "W" shape with the middle peak at midday (1200–1300 LT). The two valleys are in the early morning (0630–0850 LT) and in the late afternoon (1745–1910 LT). $\Delta T_{B,STD}$ had a similar trend except that the absolute value is about from one fifth to one half of $\Delta T_{B,AVG}$, indicating that the azimuth angular effect should be considered especially around midday. This varying pattern is controlled mainly by soil moisture, solar radiation, and LAI. Another interesting finding in this study is that the $\Delta T_{B,AVG}$ has a good relation to soil surface net radiation. A major influence controlling the water loss from irrigated crops is the net radiation intensity [*Linacre*, 1968]; thus, $\Delta T_{B,AVG}$ in turn can be used to predict soil moisture content.

Notation

(θ, φ) view zenith and azimuth angles, degree.
(θ_s, φ_s) solar zenith and azimuth angles, degree.
T_a air temperature at 2 m height, Celsius degree.
u wind speed at 2 m height, m/s.
w_s soil surface volume water content, %.

h_a air humidity at 2 m height, mb.
R_{tot} daily total solar radiation of 1 day, MJ m^{-2} d^{-1}.
R_{sun} solar total radiation at the top of canopy, W m^{-2}.
$R_{n,soil}$ soil surface net radiation (W m^{-2}).
$T_B(\theta)$ directional brightness temperature at view zenith angle θ.
$T_B(\theta, \varphi)$ directional brightness temperature at view zenith angle θ, and view azimuth angles φ.
$\Delta T_B(\theta, \varphi)$ brightness temperature difference between nadir and off nadir: $T_B(0) - T_B(\theta, \varphi)$.
$\Delta T_{B,AVG}$ mean $\Delta T_B(\theta, \varphi)$ for all view azimuth at view zenith angle 55.
$\Delta T_{B,STD}$ standard deviation of $\Delta T_B(\theta, \varphi)$ for all view azimuth at view zenith angle 55.
$\Delta T_{B,MAX}$ daily maximum $\Delta T_{B,AVG}$.
LAI crop leaf area index (m^2 m^{-2}).
SPP solar principal plane.
CPP cross solar principal plane.
VIS visible spectral range.
NIR near infrared range.
TIR thermal infrared range.
MELS modified extended L systems.
DOY day of year (Julian day).

[63] **Acknowledgments.** This work was supported by the Chinese Natural Science Foundation Project (40801135 and 40730525), China's Special Funds for Major State Basic Research Project (2007CB714402), and the Fundamental Research Funds for the Central Universities. We wish to thank the authors of the 4SAIL and DART models for providing us with the programs for comparison and the reviewers for providing useful comments.

References

Balick, L. E., and B. A. Hutchinson (1986), Directional thermal infrared exitance distributions from a leafless deciduous forest, *IEEE Trans. Geosci. Remote Sens.*, *GE-24*, 693–698, doi:10.1109/TGRS.1986.289616.

Balick, L. K., B. A. Hutchinson, J. A. Smith, and M. J. McGuire (1987), Directional thermal exitance distributions of a deciduous forest in summer, *IEEE Trans. Geosci. Remote Sens.*, *GE-25*, 410–412, doi:10.1109/TGRS.1987.289824.

Bastiaanssen, W. G. M., M. Menenti, R. A. Feddes, and A. A. M. Holtslag (1998), A remote sensing surface energy balance algorithm for land (SEBAL). 1. Formulation, *J. Hydrol.*, *198*, 212–213.

Belot, A., J.-P. Gastellu-Etchegorry, and A. Perrier (2004), A 3D model of mass and energy transfers in vegetated canopy, paper presented at 26th Conference on Agricultural and Forest Meteorology, Am. Meteorol. Soc., Vancouver, B. C., Canada.

Chehbouni, A., Y. Nouvellon, J. P. Lhomme, C. Watts, G. Boulet, Y. H. Kerr, M. S. Moran, and D. C. Goodrich (2001a), Estimation of surface sensible heat flux using dual angle observations of radiative surface temperature, *Agric. For. Meteorol.*, *108*, 55–65, doi:10.1016/S0168-1923(01)00221-0.

Chehbouni, A., Y. Nouvellon, Y. H. Kerr, M. S. Moran, C. Watts, L. Prevot, D. C. Goodrich, and S. Rambal (2001b), Directional effect on radiative surface temperature measurements over a semiarid grassland site, *Remote Sens. Environ.*, *76*, 360–372, doi:10.1016/S0034-4257(01)00183-3.

Chen, L., Q. H. Liu, and W. Fan (2002), A bi-directional gap model for simulating the directional thermal radiance of row crops, *Sci. China, Ser. D*, *45*, 1087–1098, doi:10.1360/02yd9106.

Choudhury, B. J., R. J. Reginato, and S. B. Idso (1986), An analysis of infrared temperature observations over wheat and calculation of latent heat flux, *Agric. For. Meteorol.*, *37*, 75–88, doi:10.1016/0168-1923(86)90029-8.

Dozier, J., and S. G. Warren (1982), Effect of viewing angle on the infrared brightness temperature of snow, *Water Resour. Res.*, *18*, 1424–1434, doi:10.1029/WR018i005p01424.

Du, Y., Q. H. Liu, L. Chen, Q. Liu, and T. Yu (2007), Modeling directional brightness temperature of the winter wheat canopy at the ear stage, *IEEE Trans. Geosci. Remote Sens.*, *45*, 3721–3739, doi:10.1109/TGRS.2007.903401.

Flerchinger, G. N., W. P. Kustas, and M. A. Weltz (1998), Simulating surface energy fluxes and radiometric surface temperatures for two arid vegetation communities using the SHAW model, *J. Appl. Meteorol.*, *37*, 449–460, doi:10.1175/1520-0450(1998)037<0449:SSEFAR>2.0.CO;2.

François, C. (2002), The potential of directional radiometric temperatures for monitoring soil and leaf temperature and soil moisture status, *Remote Sens. Environ.*, *80*, 122–133, doi:10.1016/S0034-4257(01)00293-0.

François, C., L. Ottlé, and L. Prévot (1997), Analytical parameterization of canopy directional emissivity and directional radiance in the thermal infrared: Application on the retrieval of soil and foliage temperatures using two directional measurements, *Int. J. Remote Sens.*, *18*, 2587–2621, doi:10.1080/014311697217495.

Fuchs, M., E. T. Kanemasu, J. P. Kerr, and C. B. Tanner (1967), Effect of viewing angle on canopy temperature measurements with infrared thermometers, *Agron. J.*, *59*, 494–496, doi:10.2134/agronj1967.00021962005900050040x.

Gastellu-Etchegorry, J. P. (2008), 3D modeling of satellite spectral images, radiation budget and energy budget of urban landscapes, *Meteorol. Atmos. Phys.*, *102*(3–4), 187–207, doi:10.1007/s00703-008-0344-1.

Guillevic, P., J. P. Gastellu-Etchegorry, J. Demarty, and L. Prévot (2003), Thermal infrared radiative transfer within three-dimensional vegetation covers, *J. Geophys. Res.*, *108*(D8), 4248, doi:10.1029/2002JD002247.

Huang, H. G., X. Z. Xin, Q. H. Liu, Q. Liu, L. F. Chen, and X. W. Li (2006), Modeling soil component temperature distribution by extending Cupid model, paper presented at International Geoscience and Remote Sensing Symposium, Inst. of Electr. and Electron. Eng., Denver, Colo.

Huang, H. G., Q. H. Liu, Q. Liu, Q. Xiao, and L. F. Chen (2007), Using multidirectional thermal images to obtain canopy component temperature and directional brightness temperature, *J. Beijing Normal Univ. Nat. Sci.*, *43*(3), 292–297.

Huang, H. G., Q. H. Liu, and W. H. Qin (2010), Thermal emission hot spot effect of crop canopies—Part I: Simulation, *IEEE J. Sel. Top. Appl. Earth Obs. Remote Sens.*, *3*(3), 313–322(JSTARS), doi:10.1109/JSTARS.2010.2046625.

Humes, K. S., W. P. Kustas, M. S. Moran, W. D. Nichols, and M. A. Weltz (1994), Variability of emissivity and surface temperature over a sparsely vegetated surface, *Water Resour. Res.*, *30*, 1299–1310, doi:10.1029/93WR03065.

Jackson, R. D., R. J. Reginati, and S. B. Idso (1977), Wheat canopy temperature: A practical tool for evaluating water requirements, *Water Resour. Res.*, *13*, 651–662, doi:10.1029/WR013i003p00651.

Jackson, R. D., R. J. Reginato, P. J. Printer Jr., and S. B. Idso (1979), Plant canopy information extraction from composite scene of row crops, *Appl. Opt.*, *18*, 3775–3782.

Kimes, D. S. (1983), Remote sensing of row crop structure and component temperatures using directional radiometric temperatures using directional radiometric temperatures and inversion techniques, *Remote Sens. Environ.*, *13*, 33–55, doi:10.1016/0034-4257(83)90026-3.

Kimes, D. S., and J. A. Kirchner (1983), Directional radiometric measurements of row crop temperatures, *Int. J. Remote Sens.*, *4*, 299–311, doi:10.1080/01431168308948548.

Kimes, D. S., S. B. Idso, J. P. J. Pinter, R. J. Reginato, and R. D. Jackson (1980), View angle effects in the radiometric measurement of plant canopy temperatures, *Remote Sens. Environ.*, *10*, 273–284, doi:10.1016/0034-4257(80)90087-5.

Kustas, W., and M. Anderson (2009), Advances in thermal infrared remote sensing for land surface modeling, *Agric. For. Meteorol.*, *149*(12), 2071–2081, doi:10.1016/j.agrformet.2009.05.016.

Kustas, W. P., and J. M. Norman (1999), Evaluation of soil and vegetation heat flux predictions using a simple two-source model with radiometric temperatures for partial canopy cover, *Agric. For. Meteorol.*, *94*, 13–29, doi:10.1016/S0168-1923(99)00005-2.

Lagouarde, J. P., Y. H. Kerr, and Y. Brunet (1995), An experimental study of angular effects on surface temperature for various plant canopies and bare soils, *Agric. For. Meteorol.*, *77*, 167–190, doi:10.1016/0168-1923(95)02260-5.

Lagouarde, J. P., H. Ballans, P. Moreau, D. Guyon, and D. Coraboeuf (2000), Experimental study of brightness surface temperature angular variations of maritime pine (Pinus Pinaster) stands, *Remote Sens. Environ.*, *72*, 17–34, doi:10.1016/S0034-4257(99)00085-1.

Lagouarde, J. P., P. Moreau, M. Irvine, J.-M. Bonnefond, J. A. Voogt, and F. Solliec (2004), Airborne experimental measurements of the angular variations in surface temperature over urban areas: Case study of Marseille (France), *Remote Sens. Environ.*, *93*, 443–462, doi:10.1016/j.rse.2003.12.011.

Li, Z.-L., R. H. Zhang, X. M. Sun, H. B. Su, X. Z. Tang, Z. L. Zhu, and J. A. Sobrino (2004), Experimental system for the study of the directional thermal emission of natural surfaces, *Int. J. Remote Sens.*, *25*, 195–204, doi:10.1080/0143116031000116453.

Linacre, E. T. (1968), Estimating the net-radiation flux, *Agric. Meteorol.*, *5*(1), 49–63, doi:10.1016/0002-1571(68)90022-8.

Liu, Q. H., X. F. Gu, and X. Li (2000), Study on thermal infrared emission directionality over crop canopies with TIR camera imagery, *Sci. China, Ser. E*, *43*, 95–103.

Liu, Q. H., Q. Liu, X. Z. Xin, R. R. Deng, G. L. Tian, L. F. Chen, J. D. Wang, and X. W. Li (2001), Experimental study on directionality in thermal infrared observations of corn canopy, paper presented at International Geoscience and Remote Sensing Symposium, Inst. of Electr. and Electron. Eng., Sydney, N. S. W., Australia.

Liu, Q., L. F. Chen, Q. H. Liu, and Q. Xiao (2003), A radiation transfer model to predict canopy radiation in thermal infrared band, *Chin. J. Remote Sens.*, *7*, 161–167.

Liu, Q. H., H. G. Huang, W. Qin, K. Fu, and X. Li (2007), An extended 3-D radiosity–graphics combined model for studying thermal-emission directionality of crop canopy, *IEEE Trans. Geosci. Remote Sens.*, *45*(9), 2900–2918, doi:10.1109/TGRS.2007.902272.

Luquet, D., A. Bégué, A. Vidal, J. Dauzat, and P. Clouvel (2003), 3D simulation of directional temperature variability within a row-cotton crop: Toward an improvement of experimental crop water status monitoring using thermal infrared, *Precis. Agric.*, *4*, 297–309, doi:10.1023/A:1024956607653.

Luquet, D., A. Vidal, J. Dauzat, A. Bégué, A. Olioso, and P. Clouvel (2004), Using directional TIR measurements and 3D simulations to assess the limitations and opportunities of water stress indices, *Remote Sens. Environ.*, *90*, 53–62, doi:10.1016/j.rse.2003.09.008.

Mauser, W., and S. Schadlich (1998), Modelling the spatial distribution of evapotranspiration on different scales using remote sensing data, *J. Hydrol.*, *212–213*, 250–267, doi:10.1016/S0022-1694(98)00228-5.

McAtee, B. K., A. J. Prata, and M. J. Lynch (2003), The angular behavior of emitted thermal infrared radiation (8–12 mum) at a semiarid site, *J. Appl. Meteorol.*, *42*, 1060–1071, doi:10.1175/1520-0450(2003)042<1060:TABOET>2.0.CO;2.

Menenti, M., L. Jia, Z.-L. Li, V. Djepa, J. Wang, M. P. Stoll, Z. Su, and M. Rast (2001), Estimation of soil and vegetation temperatures with multiangular thermal infrared observations: IMGRASS, HEIFE, and SGP 1997 experiments, *J. Geophys. Res.*, *106*, 11,997–12,010, doi:10.1029/2000JD900671.

Merlin, O., and A. Chehbouni (2004), A different approaches in estimating heat flux using dual angle observations of radiative surface temperature, *Int. J. Remote Sens.*, *25*, 275–289, doi:10.1080/0143116031000116408.

Monteith, J. L., and G. Szeicz (1962), Radiative temperature in the heat balance of natural surfaces, *Q. J. R. Meteorol. Soc.*, *88*, 496–507, doi:10.1002/qj.49708837811.

Moran, M. S., T. R. Clarke, Y. Inoue, and A. Vidal (1994), Estimating crop water deficit using the relation between surface-air temperature and spectral vegetation index, *Remote Sens. Environ.*, *49*, 246–263, doi:10.1016/0034-4257(94)90020-5.

Noilhan, J., and J. F. Mahfouf (1996), The ISBA land surface parameterisation scheme, *Global Planet. Change*, *13*, 145–159, doi:10.1016/0921-8181(95)00043-7.

Norman, J. M. (1979), Modeling the complete crop canopy, in *Modification of the Aerial Environment of Crops*, edited by B. J. Barfield, J. Gerber, and S. Joseph, pp. 249–277, Am. Soc. of Agric. Eng., St. Joseph, Mich.

Norman, J. M. (1982), Simulation of microclimates, in *Biometeorology in Integrated Pest Management*, edited by J. L. Hatfield and I. J. Thomason, pp. 65–99, Academic, New York.

Norman, J. M., J.-L. Chen, and N. Goel (1990), Thermal emissivity and infrared temperature dependence on plant canopy architecture and view angle, paper presented at International Geoscience and Remote Sensing Symposium, Inst. of Electr. and Electron. Eng., College Park, Md.

Norman, J. M., W. P. Kustas, J. H. Prueger, and G. R. Diak (2000), Surface flux estimation using radiometric temperature: A dual-temperature-difference method to minimize measurement errors, *Water Resour. Res.*, *36*, 2263–2274, doi:10.1029/2000WR900033.

Parsons, A. J. (1985), Directionality in emitted infrared radiation from grassy surfaces, *Int. J. Remote Sens.*, *6*, 903–910, doi:10.1080/01431168508948513.

Paw U, K. T. (1991), Anisotropy of thermal infrared exitance above and within plant canopies, *Eur. Space Agency Spec. Publ.*, *ESA-SP-319*, 369–374.

Paw U, K. T. (1992), Development of models for thermal infrared radiation above and within plant canopies, *ISPRS J. Photogramm. Remote Sens.*, *47*, 189–203, doi:10.1016/0924-2716(92)90032-5.

Paw U, K. T., S. L. Ustin, and C. A. Zhang (1989), Anisotropy of thermal infrared exitance in sunflower canopies, *Agric. For. Meteorol.*, *48*, 45–58.

Qin, W., and S. A. W. Gerstl (2000), 3-D scene modeling of semidesert vegetation cover and its radiation regime, *Remote Sens. Environ.*, *74*, 145–162, doi:10.1016/S0034-4257(00)00129-2.

Rivas, R., and V. Caselles (2004), A simplified equation to estimate spatial reference evaporation from remote sensing-based surface temperature and local meteorological data, *Remote Sens. Environ.*, *93*, 68–76, doi:10.1016/j.rse.2004.06.021.

Sánchez, J. M., V. Caselles, and W. P. Kustas (2008), Estimating surface energy fluxes using a micro-meteorological model and satellite images, *Tethys J. Weather Clim. West. Mediterr.*, *5*, 25–36.

Saux-Picart, S., C. Ottlé, A. Perrier, B. Decharme, B. Coudert, M. Zribi, N. Boulain, and B. Cappelaere (2009), SEtHyS_Savannah: A multiple source land surface model applied to sahelian landscapes, *Agric. For. Meteorol.*, *149*, 1421–1432, doi:10.1016/j.agrformet.2009.03.013.

Seguin, B., D. Courault, and M. Guerif (1994), Surface temperature and evapotranspiration: Application of local scale methods to regional scales using satellite data, *Remote Sens. Environ.*, *49*, 287–295, doi:10.1016/0034-4257(94)90023-X.

Smith, J. A., R. Jerrell, J. Ballard, and J. A. Pedelty (1997a), Effect of three-dimensional canopy architecture on thermal infrared exitance, *Opt. Eng.*, *36*, 3093–3100, doi:10.1117/1.601527.

Smith, J. A., N. S. Chauhan, T. J. Schmugge, and J. R. Ballard Jr. (1997b), Remote sensing of land surface temperature: The directional viewing effect, *IEEE Trans. Geosci. Remote Sens.*, *35*, 972–974, doi:10.1109/36.602539.

Sobrino, J., and V. Caselles (1990), Thermal infrared radiance model for interpreting the directional radiometric temperature of a vegetative surface, *Remote Sens. Environ.*, *33*, 193–199, doi:10.1016/0034-4257(90)90030-P.

Timmermans, J., W. Verhoef, C. van der Tol, and Z. Su (2009), Retrieval of canopy component temperatures through Bayesian inversion of directional thermal measurements, *Hydrol. Earth Syst. Sci.*, *13*, 1249–1260, doi:10.5194/hess-13-1249-2009.

van der Tol, C., W. Verhoef, J. Timmermans, A. Verhoef, and Z. Su (2009), An integrated model of soil-canopy spectral radiances, photosynthesis, fluorescence, temperature and energy balance, *Biogeosciences*, *6*, 3109–3129.

Verhoef, W., L. Jia, Q. Xiao, and Z. Su (2007), Unified optical-thermal four-stream radiative transfer theory for homogeneous vegetation canopies, *IEEE Trans. Geosci. Remote Sens.*, *45*, 1808–1822, doi:10.1109/TGRS.2007.895844.

Xiao, Q., Q. H. Liu, X. W. Li, L. F. Chen, Q. Liu, and X. Z. Xin (2003), A field measurement method of spectral emissivity and research on the feature of soil thermal infrared emissivity, *J. Infrared Millimeter Waves*, *22*, 373–378.

Yan, G., M. Friedl, X. Li, J. Wang, C. Zhu, and A. Strahler (2001), Modeling directional effects from nonisothermal land surfaces in wide band thermal infrared measurements, *IEEE Trans. Geosci. Remote Sens.*, *39*, 1095–1099, doi:10.1109/36.921427.

Yan, G., L. Jiang, J. Wang, L. Chen, and X. Li (2003), Thermal bidirectional gap probability model for row crop canopies and validation, *Sci. China, Ser. D*, *46*, 1241–1249.

Yu, T., X. Gu, G. Tian, M. Legrand, F. Baret, J.-F. Hanocq, R. Bosseno, and Y. Zhang (2004), Modeling directional brightness temperature over a maize canopy in row structure, *IEEE Trans. Geosci. Remote Sens.*, *42*, 2290–2304, doi:10.1109/TGRS.2004.834196.

Y. Du, X. Li, Q. Liu, and W. Qin, State Key Laboratory of Remote Sensing Science, Institute of Remote Sensing Applications, Chinese Academy of Sciences, Beijing Normal University, Beijing 100101, China.

H. Huang, Key Laboratory for Silviculture and Conservation of Ministry of Education, Beijing Forestry University, Beijing 100083, China. (huaguo.huang@gmail.com)